Flexible
Elektrische
Netze

FINAL PROJECT REPORT

Center for FEN

Electromagnetic Interference of Medium Voltage AC and DC Overhead Lines and Cables

Seed Fund Project MV 04

Flexible Elektrische Netze

Final Project Report

Seed Fund Project MV 04

Electromagnetic Interference of Medium Voltage AC and DC Overhead Lines and Cables

Conducted by

Univ.-Prof. Antonello Monti, Ph.D.
Institut für Automation of Complex Power Systems
der Rheinisch-Westfälischen Technischen Hochschule Aachen

and

Univ.-Prof. Dr.-Ing. Albert Moser
Institut für Elektrische Anlagen und Energiewirtschaft
der Rheinisch-Westfälischen Technischen Hochschule Aachen

In collaboration with
Robert Uhl, M.Sc.
Julian Lichtinghagen, Wirt.-Ing. M.Sc.

Mathieustr. 10
52074 Aachen

post_acs@eonerc.rwth-aachen.de

Tel.: +49 241 80 49700
Fax: +49 241 80 49709

Content

1 Background and Objectives of the Study 3
2 Analysis and Modeling 4
2.1 Coupling Mechanisms 4
2.1.1 Corona Discharges in Medium Voltage Grids 7
2.2 Summary of Analysis Concerning Coupling Mechanisms 12
2.3 Modeling of Transmission Lines 13
2.3.1 Calculation of the System Impedance and Admittance Matrices 14
2.4 Solution Techniques for the Transmission Line Model 15
3 Exemplary Calculations 16
3.1 Arrangements to be analyzed 16
3.2 Parameters of the Exemplary Arrangements 20
3.3 Results of Steady-state and Transient Analysis 24
3.3.1 Steady-state Results 24
3.3.2 Summary of the Steady-state Results 29
3.3.3 Transient Results for Arrangements with AC Conductors only 30
3.3.4 Summary of Transient Results for AC 40
3.3.5 Transient Results for Arrangements with DC Conductors only 41
3.3.6 Summary of Transient Results for DC 50
4 Influence of Injected Currents and Induced Voltages on other Operating Resources 51
4.1 Power Transformers under DC Bias 51
4.2 Instrument Transformers under DC Bias 54
4.3 Effects on Converter 54
4.4 Mitigation Options 55
5 Conclusion, Outlook and Future Work 56
6 Bibliography 59
7 List of Tables and Figures 62

1 Background and Objectives of the Study

Both overhead lines and cables, which run parallel to each other, cause mutual electromagnetic interference (EMI). Due to these interferences, violations of the EMI directives can occur, which may result in limitations for the operation and expansion of transmission and distribution grids. During a transition process from AC to DC or hybrid medium voltage grids, there may be a parallel operation of AC and DC systems. Hence, there could be AC and DC medium voltage overhead lines and cables in operation that run parallel to each other (hybrid lines). For this reason, it is necessary to determine the mutual electromagnetic interference of AC and DC medium voltage lines, to consider possible restrictions during network operation and planning.

On the one hand, in AC grids injected DC currents due to electromagnetic interference cause premagnetization of transformers. This can lead to higher losses, increased noise emissions and an inadmissible heating of the transformers. In extreme cases, this may even result in the destruction of transformers. Additionally, malfunctions of protection devices may occur, due to a premagnetization of the instrument transformers. Therefore, it might be necessary to verify the functionality of the AC protection system for hybrid lines. On the other hand, the effects of AC currents being injected in DC grids also need to be investigated, especially their effect on converters.

Therefore, the aim of this project is to analyze and evaluate the mutual electromagnetic interference of AC and DC medium voltage lines. For this purpose in a first step, existing methods and examinations regarding the EMI between extra-high voltage and high voltage overhead lines are analyzed. Based on the analysis of the different possible coupling mechanisms that cause EMI, it is decided which coupling mechanisms need to be considered for medium voltage lines. Afterwards the used line models for steady state and transient EMI calculations are described. In exemplary calculations the steady state and transient EMI for different arrangements are investigated. Finally, the effects of the calculated EMI on AC and DC operating resources, like power transformers, instrument transformers and converters, are pointed out.

2 Analysis and Modeling

In this chapter the different possible coupling mechanisms are analyzed. Based on the results of the analysis it is decided which coupling mechanisms have to be considered for EMI calculations in medium voltage AC and DC grids. In this context, a distinction between steady state and transient conditions is made. Overhead lines and cables are distinguished in their behavior in terms of EMI as well. After the analysis of the coupling mechanisms the used line models for steady state conditions and for transient conditions are summarized. Finally, the solution methods for both steady state and transient EMI calculations are outlined.

2.1 Coupling Mechanisms

The mutual interference between different conductors results from three coupling mechanisms.

- Capacitive coupling, caused by electric fields resulting from line-to-earth-voltages
- Inductive coupling, caused by magnetic fields resulting from phase currents
- Conductive coupling, caused by flux fields through a common impedance of two circuits

Capacitive Coupling

The capacitive coupling is frequency-dependent and rises with increasing frequency. Therefore, DC lines only cause very low capacitive coupling in steady state conditions [1, 2]. Hence, the capacitive coupling caused by DC lines in steady state conditions can be neglected for EMI calculations. On the other hand, the capacitive coupling caused by AC lines with an operating frequency of 50 Hz needs to be further analyzed. Because of the low electrical conductivity of air, an electric field spreads out between two overhead lines with different voltages. In contrast, the electric field caused by a cable is shielded due to grounded cable shielding and the much higher electric conductivity of soil compared to air. Therefore, the capacitive coupling is only relevant for the mutual electromagnetic interference between overhead lines. The mutual capacitive coupling of two overhead lines strongly depends on their distance. Figure 1 shows the percentage decrease of steady state capacitive interference of two medium-voltage overhead lines with increasing distance. The capacitive interference on line I_1 caused by the three phase AC circuit 1 ($U_1V_1W_1$) at a distance of 0.5 meters between I_1 and W_1 is set as reference point

(100 %). The overhead lines are placed at a height of 15 meters above the ground with the assumption that the conductor's sag is already taken into account in this height. The line-to-line RMS voltage of circuit 1 is 20 kV (symmetrical) and the frequency is assumed to be 50 Hz.

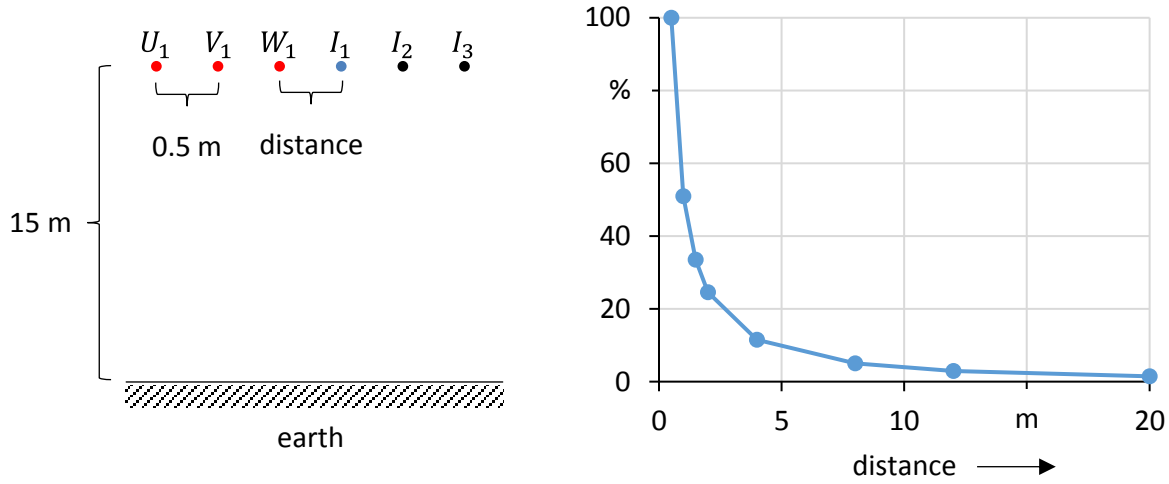

Figure 1: Capacitive interference on line I_1 caused by circuit 1 depending on the distance between I_1 and W_1

As shown in Figure 1, the capacitive interference decreases strongly with increasing distance. For the examined arrangement, there is nearly no capacitive interference for a distance larger than 20 meters. Hence, capacitive coupling has only to be considered for overhead lines that run parallel to each other within a distance of 20 meters.

Inductive Coupling

The inductive coupling is also frequency-dependent and strongly rises with increasing frequency. According to the law of electromagnetic induction, a constant magnetic field does not induce voltages. Therefore, there is no inductive interference caused by DC lines in steady state conditions. Contrary to the electric field a cable shielding and the soil do not shield magnetic fields. Hence, inductive interference has to be considered for both AC overhead lines and AC cables as well as DC during transients.

The mutual inductive coupling between two conductors also depends on their distance. Figure 2 shows the percentage decrease of steady state inductive interference for the same arrangement as shown in Figure 1. The phase RMS currents of the three phase AC circuit 1 are set to 500 A (symmetrical) at a frequency of 50 Hz.

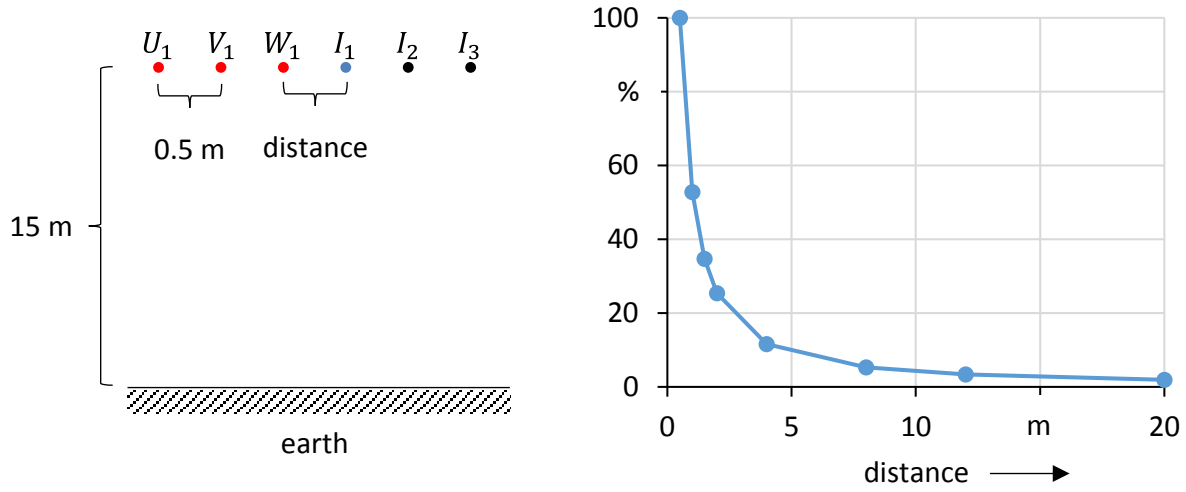

Figure 2: Inductive interference on line I_1 caused by circuit 1 depending on the distance between I_1 and W_1

As can be seen in Figure 2, the inductive interference decreases as strong as the capacitive coupling with increasing distance. For the shown arrangement, there is almost no inductive interference for a distance larger than 20 meters. Hence, inductive coupling has only to be considered for overhead lines that run parallel to each another within a distance of 20 meters.

Conductive Coupling

Conductive coupling occurs when different circuits have a common impedance. This situation is unlikely for AC circuits, because it only happens in fault conditions. Either for a short circuit between two different circuits or simultaneous earth faults, which are both unlikely. Therefore, conductive coupling caused by AC circuits is neglected in this project.

In contrast to AC circuits, DC circuits can cause conductive coupling in normal operation conditions. This happens if a high-impedance transmission channel is formed due to corona discharges on the surface of the conductors of overhead lines. Thus, conductive coupling caused by DC circuits only occurs if corona discharges take place on the conductors' surface. For this reason, it has to be investigated thoroughly if corona discharges appear at aerial conductors in medium voltage DC grids[1]. Due to the surrounding insulation layers, no corona discharges can occur at the surface of the current carrying conductors of DC cables.

[1] Short circuits between two different systems and simultaneous earth faults of two different systems are neglected due to the low probability.

2.1.1 Corona Discharges in Medium Voltage Grids

If the electrical field strength at the surface of an aerial DC conductor reaches approximately 30 kV/cm, corona discharges occur [3]. In extra-high voltage and high voltage grids, corona discharges are a well-known phenomenon. Subject to this analysis is, whether corona discharges also occur at lower voltage levels.

Arrangement with two DC conductors

As a first simple case to consider, the conductor arrangement shown in Figure 3 is investigated. The maximum field strength of a given conductor arrangement can be estimated by means of the utilization factor according to Schwaiger. The utilization factor η indicates the ratio between the maximum field strength E_{max} of a given conductor arrangement and the field strength E_0 inside an ideal parallel-plate capacitor with the same electrode distance [3]. If η is known for a conductor arrangement, E_{max} can be derived with Formula 2.1.

$$E_{max} = \frac{1}{\eta} \cdot E_0 \tag{2.1}$$

The smaller η, the more inhomogeneous is the electric field. To estimate the maximum field strength for medium voltage DC overhead lines the conductor arrangement shown in Figure 3 is investigated.

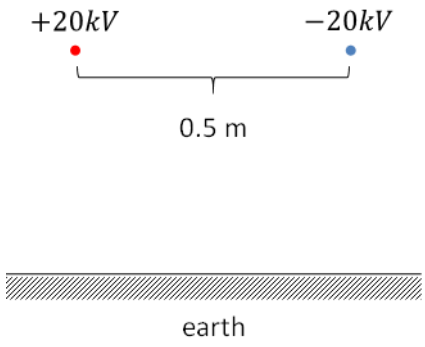

Figure 3: Investigated DC overhead line arrangement

The field strength E_0 inside an ideal parallel-plate capacitor is given by Formula 2.2.

$$E_0 = \frac{U}{d} \tag{2.2}$$

With Formula 2.2 the field strength E_0 for the examined conductor arrangement results in

$$\frac{U}{d} = \frac{+20kV - (-20kV)}{0.5m} = \frac{40kV}{0.5m} = 0.8\ \frac{kV}{cm}$$

To reach maximum field strength of $30\ \frac{kV}{cm}$ the utilization factor η needs to be smaller than

$$\frac{E_0}{E_{max}} = \frac{0.8}{30} = 0.02\overline{6}$$

The utilization factor for different arrangements can be found in the literature. It depends on the parameters p and q, which are based on the geometric data r, R and s of cylindrical arrangements, shown in Figure 4.

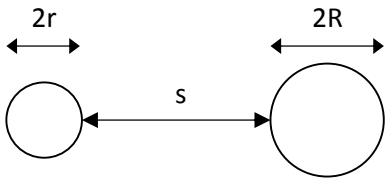

Figure 4: Input parameters for the calculation of p and q

This input parameters p and q are calculated by Formula 2.3 and Formula 2.4.

$$p = \frac{r + s}{r} \tag{2.3}$$

$$q = \frac{R}{r} \tag{2.4}$$

For two typical medium voltage overhead line conductors with a radius of 2 centimeters and a distance of 0.5 meters, p is equal to

$$p = \frac{0.02+0.5}{0.02} = 26,$$

while q is equal to

$$q = \frac{0.02}{0.02} = 1.$$

Table 1 shows the utilization factor for a cylinder arrangement with q equal to one and a variation of p.

P	Utilization factor for $q = 1$
1	1
2	0.861
4	0.684
8	0.497
10	0.442
20	0.291
50	0.1574
100	0.094
1000	0.0138

Table 1: Utilization factor depending on parameters p and q

According to Table 1, the utilization factor for the given arrangement is approximately 0.291 (p=20). This is one magnitude higher than the necessary utilization factor of $0.02\overline{6}$, which is needed for corona discharges to take place. It also has to be considered that local increases of the electric field strength can occur due to imperfections on the conductor surface. As shown before, these local increases need to result in a 10 times higher electric field strength, so that corona discharges occur. Imperfections on the conductor surface appear rather seldom, thus, there occur no or only negligible corona discharges for the considered, simple medium voltage overhead line arrangement.

Arrangement with more than two DC conductors

For more than two DC conductors or for consideration of additional AC conductors in the conductor arrangement, the previously shown estimation by usage of the utilization factor according to Schwaiger cannot be used. Therefore, in this section an appropriate way to calculate the electrical field strength at the conductor's surface is shown [4].

For medium voltage overhead transmission lines, normally no bundled conductors are used [5]. Further it is assumed that the cylindrical conductors have an infinite length and run parallel for the whole distance in a space-charge free environment. The conductor's sag is converted into a mean height and a possible influence of the towers is neglected. The earth is assumed to be flat and is modelled as equipotential surface with zero potential and infinite conductivity. For real arrangements the condition that the conductor's height is much larger than the conductor's radius is fulfilled.

The charge at each conductor's surface is modelled as a line charge in the center of the particular conductor. A potential coefficient matrix $\boldsymbol{P}$ is built from the geometrical arrangement consisting of the considered conductors as shown in Formulas 2.5 and 2.6 utilizing the method of mirror charges. In this formulas, x_k is the horizontal position of the conductor k, h_k is its height above the earth while r_k is its radius. d_{km} in Formula 2.7 is the distance between two conductors k and m, while D_{km} in Formula 2.8 is the distance between the conductor k and the mirror of conductor m.

$$P_{kk} = \frac{1}{2\pi\varepsilon} \cdot \ln\left(\frac{2h_k}{r_k}\right) \tag{2.5}$$

$$P_{km} = \frac{1}{2\pi\varepsilon} \cdot \ln\left(\frac{D_{km}}{d_{km}}\right) \tag{2.6}$$

$$d_{km} = \sqrt{(x_k - x_m)^2 + (h_k - h_m)^2} \tag{2.7}$$

$$D_{km} = \sqrt{(x_k - x_m)^2 + (h_k + h_m)^2} \tag{2.8}$$

The DC potentials of the conductors are assumed to be equal over the whole length of the line. They form the potential vector $\vec{U}$. By solving the system of linear equations in Formula 2.9, the vector $\vec{L}$ with the line charges for every conductor is obtained.

$$\boldsymbol{P} \cdot \vec{L} = \vec{U} \tag{2.9}$$

The electrical field vector at distance r for every conductor k can be obtained by Formula 2.10, where it is assumed that every conductor's electrical field is radial. By superimposing the influence of every conductor on the electrical field, the total electrical field can be determined.

$$\vec{E}_k = \frac{L_k}{2\pi\varepsilon \cdot r} \cdot \vec{e}_{r,k} \tag{2.10}$$

After calculating the maximum electrical field strength on the surface of every conductor, it can be examined whether the critical electrical field strength of 30 kV/cm, at which corona discharges occur, is reached.

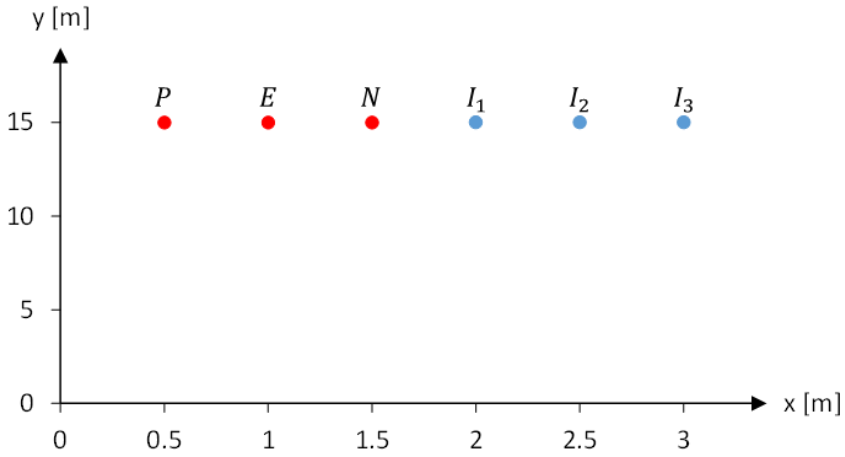

Figure 5: Conductor arrangement for analysis of DC corona discharges

For the aerial conductor arrangement shown in Figure 5 it is investigated whether DC corona discharges can occur for a more complex conductor arrangement. The positive DC conductor, P, has a potential of 25 kV while the negative conductor, N, has a potential of -25 kV. The conductor E which is the metallic return, is grounded and therefore has a potential of 0 kV. The three conductors I_1, I_2 and I_3 are assumed to be AC conductors, whose alternating field component has negligible influence on the DC corona discharges. Therefore, their potential is set to 0 kV [6]. The radius of all conductors is 0.01 m. The above shown system of linear equations is solved and the maximum electrical field strength at every conductor's surface is calculated by superimposing the resulting electrical field of all considered conductors. The resulting electrical field strength is shown in Table 2. All values are much lower than the electrical field strength of approximately 30 kV/cm, at which corona discharges take place. Therefore no or only negligible corona discharges occur, which means that the conductive coupling between medium voltage overhead lines does not need to be considered for the EMI calculations in this study.

Conductor	Maximum electrical field strength
P	5.3 kV/cm
E	0.4 kV/cm
N	5.9 kV/cm
I_1	1.1 kV/cm
I_2	0.3 kV/cm
I_3	0.1 kV/cm

Table 2: Maximum DC electrical field strengths at conductors' surface of analyzed arrangement

2.2 Summary of Analysis Concerning Coupling Mechanisms

The results of the analysis are summarized in Table 3 and Table 4. Table 3 shows the relevant coupling mechanisms for steady state EMI calculations and Table 4 for transient EMI calculations.

Coupling mechanism	AC		DC	
	Overhead line	Cable	Overhead line	Cable
Capacitive coupling	✓	×	×	×
Inductive coupling	✓	✓	×	×
Conductive coupling[2]	×	×	×	×

Table 3: Relevant coupling mechanisms between medium voltage lines in steady state conditions

[2] Short circuits between two different systems and simultaneous earth faults of two different systems are neglected, due to the low probability.

Coupling mechanism	AC		DC	
	Overhead line	Cable	Overhead line	Cable
Capacitive coupling	✓	×	✓	×
Inductive coupling	✓	✓	✓	✓
Conductive coupling	×	×	×	×

Table 4: Relevant coupling mechanisms between medium voltage lines in transient conditions

2.3 Modeling of Transmission Lines

The modeling of transmission lines like overhead transmission lines and cables with distributed parameters is based on the telegrapher's equations [7]. With this approach, travelling waves, their travel time, reflection and refraction as well as the frequency-dependence of the line's parameters are taken into account. This leads to a higher accuracy of the model, especially for transient simulations, as achieved by using an equivalent circuit with lumped parameters.

For the telegrapher's equations an infinitesimal short segment of the transmission line with the length Δx is considered, as shown in Figure 6 for a single conductor. The capacitive and inductive coupling between several conductors is modeled using an ideal current source U'·Δx and an ideal voltage source I'·Δx, respectively. Due to the infinitesimal short segment, all named values are per unit length. As the limit Δx→0, the following differential equations in the frequency domain are obtained:

$$\frac{\mathrm{dV}(x,\omega)}{\mathrm{dx}} = -\mathrm{Z}'(\omega)\cdot \mathrm{I}(x,\omega) \tag{2.11}$$

$$\frac{\mathrm{dI}(x,\omega)}{\mathrm{dx}} = -\mathrm{Y}'(\omega)\cdot \mathrm{V}(x,\omega) \tag{2.12}$$

For arrangements with more than one conductor, the system impedance matrix Z'(ω) and the system admittance matrix Y'(ω) are square matrices and V(x, ω) and I(x, ω) are vectors. Both have dimensions equal to the number of conductors. The matrices Z'(ω) and Y'(ω) are calculated based on the geometrical arrangement and some basic parameters of the considered

conductors and are highly frequency-dependent due to the skin effect in the conductors and the frequency-dependency of the earth return path.

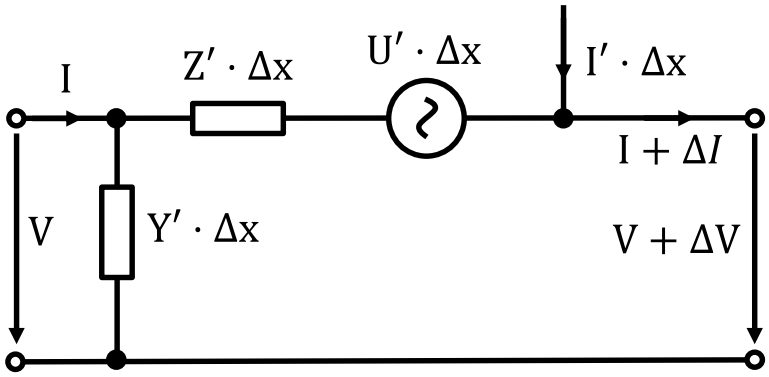

Figure 6: Equivalent circuit of infinitesimal short transmission line segment

2.3.1 Calculation of the System Impedance and Admittance Matrices

The highly frequency-dependent system impedance and admittance matrices Z'(ω) and Y'(ω) of an arrangement are calculated based on the considered frequency as well as some input parameters. These are the geometrical arrangement and basic parameters of the considered aerial conductors or buried cables as well as the ground resistivity and the relative permeability of the ground. It is assumed that the conductors form a perfectly round cylinder, as well as that the earth is flat and has a homogenous ground resistivity and permeability. For overhead lines and cables the same transmission line model, as introduced before, can be used. But there are two ways of calculating the particular system impedance and admittance matrices, depending on whether the arrangement consists of only aerial conductors, cables or cables and aerial conductors.

The calculation of the system's impedance and admittance matrices for an arrangement consisting only of aerial conductors takes the relative position of the conductors, but also the conductors' sag into account. Further, the radius of the conductors and their DC resistance per unit length are needed input parameters. The conductor's sag d_{sag} is eliminated by calculating a mean high h of the conductor based on the high h' of the conductor at the towers with Formula 2.13. Thus, a straight conductor can be assumed, which simplifies all further calculations.

$$h = h' - \frac{2}{3} \cdot d_{sag} \tag{2.13}$$

The calculation of the system impedance and admittance matrices for an arrangement consisting only of cables takes the relative position of the cables, but also the radius of their different layers into account. Further, the resistivity, relative permeability and relative permittivity of these layers are required input parameters. Arrangements with aerial conductors and cables represent a special case of cable arrangements. In this case, the aerial conductors are treated as “aerial cables” without any insulation or conductor layers, only the inner conductor, which carries the operating current, is modeled.

2.4 Solution Techniques for the Transmission Line Model

Due to the strong frequency-dependence of the transmission line model’s parameters the transmission line is modeled in the frequency domain, as shown before.

For steady-state AC-only simulations only the fundamental frequency has to be considered. Calculations with the transmission line model can easily be performed for steady-state in the frequency domain. The system impedance and admittance matrices are calculated for the fundamental frequency and are converted to the admittance matrix $\underline{Y}$ of the equivalent circuit of the considered transmission line segment under consideration of its length. For this conversion an aborted series expansion is used, utilizing a modal transformation.

To perform transient simulations, a conversion from the frequency domain to the time domain has to be done. For this conversion different solution techniques exist, which differ regarding their resulting accuracy in the time domain due to the made simplifications. The simplest one, the Bergeron transmission line model, is only precise for a single frequency, i.e. the fundamental frequency of the considered system. Much more precise is the frequency-dependent modal domain model, which takes the frequency-dependence of all parameters for a user-defined frequency range into account. Only the internal matrices for the transformation between phase and modal domain are constant, although they are actually frequency-dependent. Most precise is the frequency-dependent phase domain model, also known as the “Universal Line Model”, which provides full frequency-dependence for a user-defined frequency range. Due to the fact that in this project AC and DC circuits and their mutual couplings are considered, only the frequency-dependent transmission line models are of interest. Therefore for all transient simulations the frequency-dependent phase domain model (“Universal Line Model”) has been used.

For travelling wave transmission line models a constraint regarding the simulation time step has to be considered. It results from the fact that traveling waves propagate along the transmission line with a certain speed, which is lower than the speed of light. The condition $\tau \geq \Delta t$ has to be met, where τ is the smallest wave travel time of a transmission line and Δt is the simulation time step. Therefore, especially for short transmission lines, the simulation time step has to be adjusted regarding the minimum wave travel time, which is proportional to the length of the transmission line.

3 Exemplary Calculations

In this chapter the results of the EMI calculations for exemplary overhead line and cable arrangements are presented. On the one hand, the EMI for pure overhead line arrangements and pure cable arrangements is calculated, but on the other hand, also the EMI for mixed overhead line and cable arrangements is calculated. For every calculation it is assumed that there are influencing conductors and influenced conductors. Every arrangement has been analyzed for AC and DC as influencing conductors. Further it is assumed that the influenced conductors do not carry any operational voltages or currents. Therefore the coupled interference voltages and currents have to be superimposed with the operational voltages and currents of these conductors.

In the following section the arrangements to be analyzed are shown. After that, the input parameters for the performed calculations are presented. Finally, the results of the steady-state and transient analysis are presented and compared regarding their coincidence.

3.1 Arrangements to be analyzed

To examine the steady state and transient EMI different arrangements are considered. The examined interference route is shown in Figure 7.

Two circuits, consisting of three conductors each, run parallel to each other from point A to point M. At point M the two circuits split and run orthogonal to each other. Therefore, from point M to both endpoints E no mutual EMI between the two circuits occurs. All sections, from point A to point M and from point M to both endpoints E, have the same length of one kilometer.

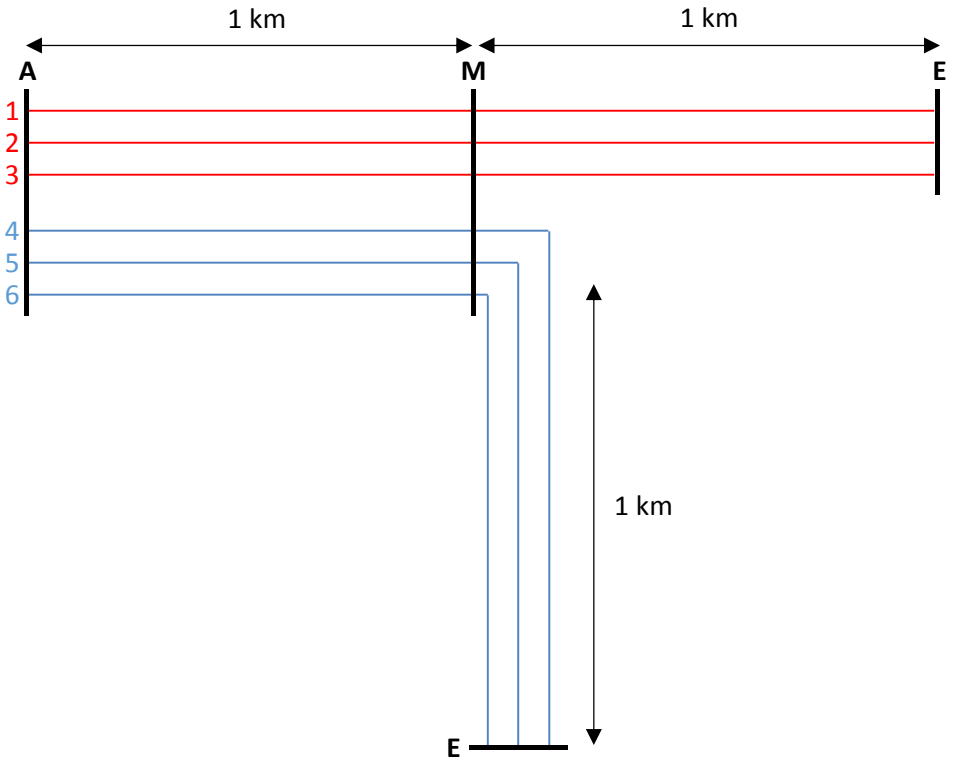

Figure 7: Examined interference route

As presented in chapter 2, overhead lines and cables differ in their behavior in terms of EMI as well as AC and DC circuits. Therefore, the EMI for eight different arrangements is calculated. These arrangements are described in Table 5.

Arrangement	Interfering circuit	Interfered circuit
AC overhead line – overhead line	overhead line (AC)	overhead line
DC overhead line – overhead line	overhead line (DC)	overhead line
AC overhead line – cable	overhead line (AC)	cable
DC overhead line – cable	overhead line (DC)	cable
AC cable – overhead line	cable (AC)	overhead line
DC cable – overhead line	cable (DC)	overhead line
AC cable – cable	cable (AC)	cable
DC cable – cable	cable (DC)	cable

Table 5: Considered arrangements

The different arrangements are shown in Figure 8 to Figure 11. The conductors causing the interference are pictured in red and the interfered conductors I_1, I_2 and I_3 are pictured in blue. The conductors of a three phase AC circuit are named U, V and W. The conductors of a bipolar DC circuit with neutral conductor are named P, E and N, where P is the positive conductor, N is the negative conductor and E is the neutral conductor. The assumed operating voltages and currents for both normal operating conditions and fault conditions are described in section 3.2. Figure 8 shows the examined arrangement consisting of two overhead line systems. Figure 9 and Figure 10 show the arrangement consisting of an overhead line system and a cable system. Figure 11 shows the arrangement consisting of two cable systems.

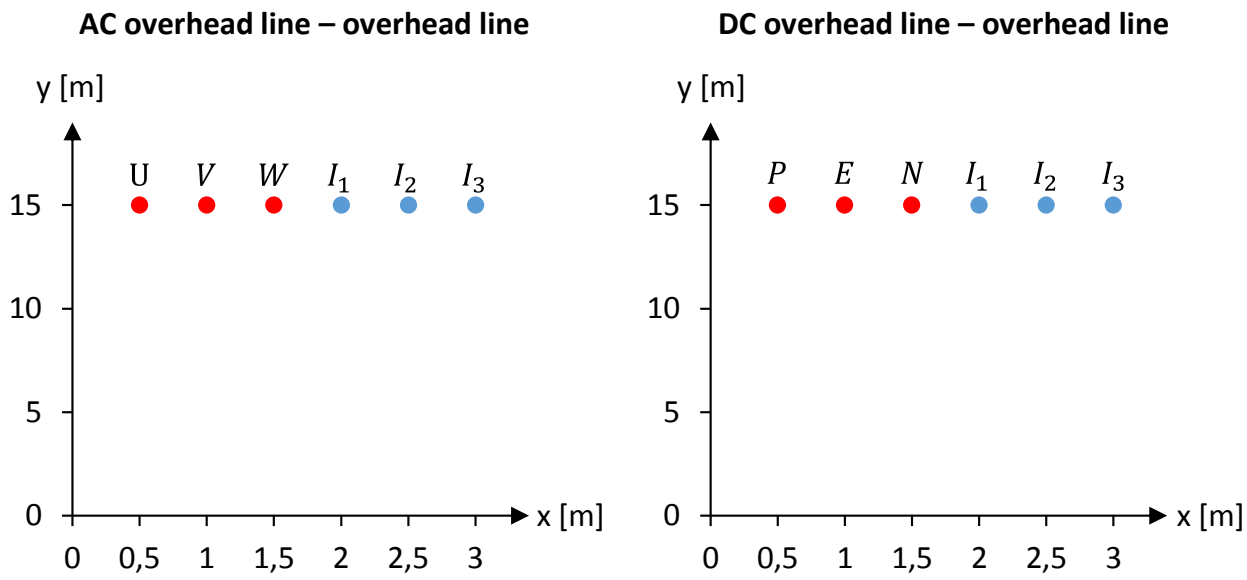

Figure 8: Overhead line – overhead line arrangements

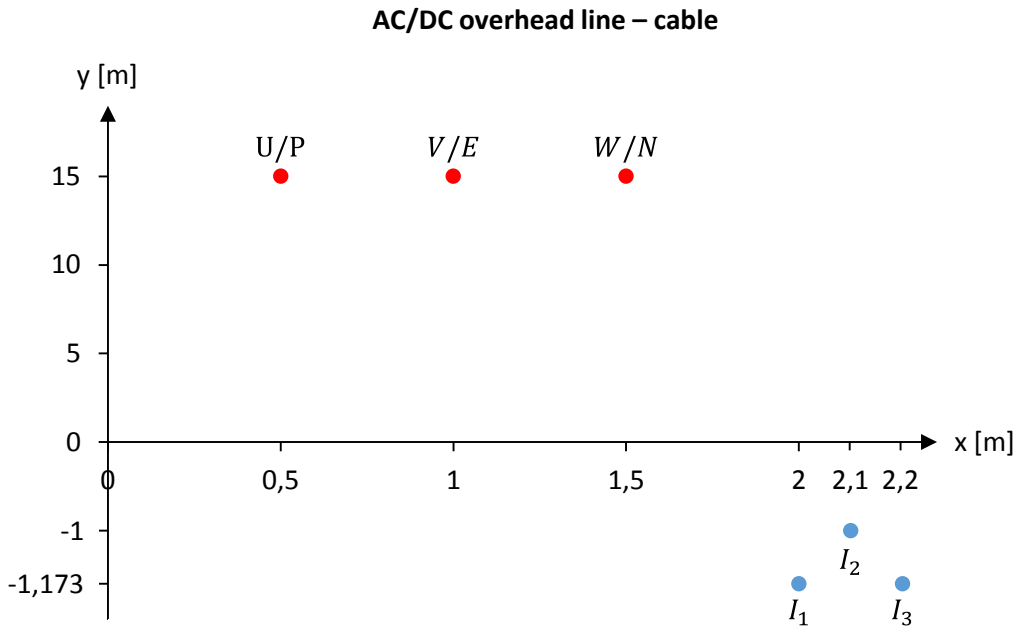

Figure 9: Overhead line – cable arrangements

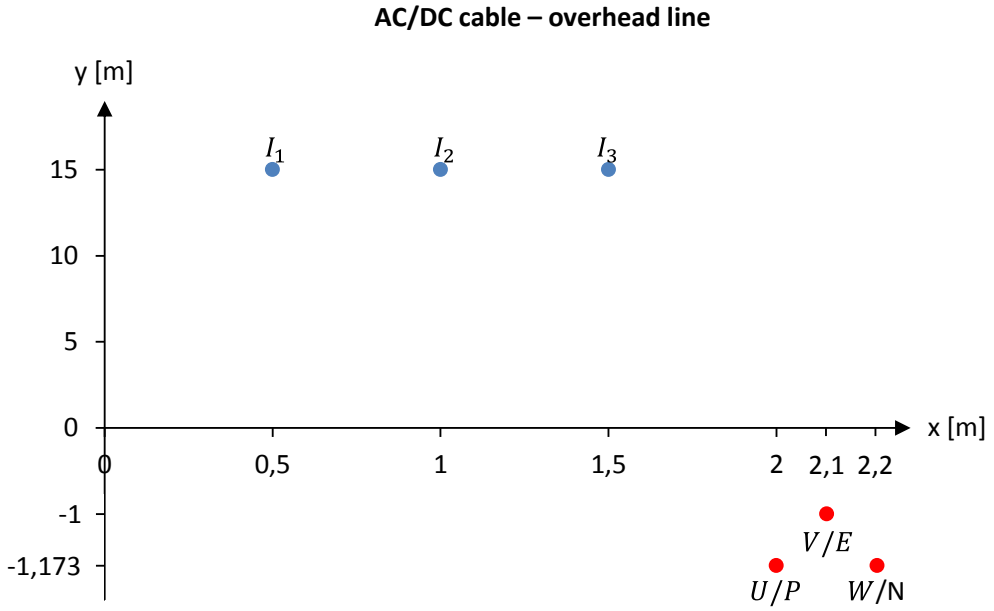

Figure 10: Cable – overhead line arrangements

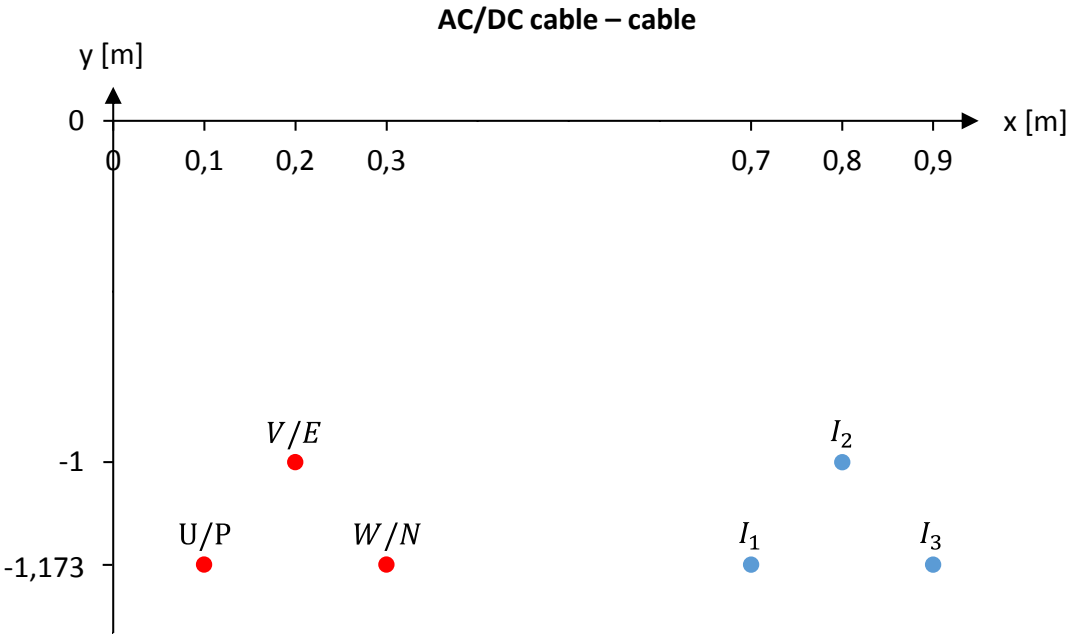

Figure 11: Cable – cable arrangements

3.2 Parameters of the Exemplary Arrangements

The parameters for all aerial conductors in the considered arrangements are shown in Table 6.

Parameter of conductor	Value
Radius	0.02 m
DC resistance per unit length	0.02 Ω/km
Conductivity per unit length	$1.0 \cdot 10^{-9}$ S/m
Relative permeability	1.0

Table 6: Parameters of the aerial conductors

All phases of the analyzed arrangements consist only of a single conductor due to the fact that in medium voltage level no bundle conductors are used. Further it is assumed that the heights of the conductors already take the conductor's sag into account. For all arrangements it is assumed that the soil resistivity is equal to 100 Ωm, which corresponds to soil consisting mainly of clay [8].

The cables in the considered arrangements consist of four layers. These are the actual conductor, carrying the current, the insulation layer, the sheath and the outer sheath/coating. The cable's sheath is ideally grounded. Table 7 shows the parameters of every layer of the considered cable with an outer diameter of 6.7 cm. It has been selected from the AC buried cable product line of a cable manufacturer under consideration of the needed AC RMS voltage and current ratings.

Layer	Parameter	Value
Conductor	Material	Aluminum (solid)
	Area	$1000\ \mathrm{mm}^2$
	Radius	$0.01905\ \mathrm{m}$
	DC resistance per unit length	$0.0291\ \Omega/\mathrm{km}$
	Specific resistance	$2.91 \cdot 10^{-8}\ \Omega\mathrm{m}$
	Relative permeability	1.0
Insulator	Material	XLPE
	Thickness	$0.00865\ \mathrm{m}$
	Relative permeability	1.0
	Relative permittivity	2.4
Conducting Sheath	Material	Copper
	Thickness	$0.0028\ \mathrm{m}$
	Specific resistance	$1.724 \cdot 10^{-8}\ \Omega\mathrm{m}$
	Relative permeability	1.0
Outer Sheath/Coating	Material	PE
	Thickness	$0.003\ \mathrm{m}$
	Relative permeability	1.0
	Relative permittivity	2.4

Table 7: Parameters of the cable layers

Regarding the parameters of the AC voltages and currents, all corresponding arrangements have been analyzed for a fundamental frequency of 50 Hz, a RMS phase-to-phase voltage of 20 kV and a RMS single line current of 0.5 kA during normal operation. A symmetrical three-phase system is supposed with no phase shift between voltages and currents, such that pure active power transmission takes place. For the analysis of fault conditions in the AC system a single-phase RMS fault current of 10 kA is considered. This fault current has been chosen due to the consideration of only single-phase faults in the exemplary calculations and the short circuit current ratings of common medium voltage circuit breakers. During the short circuit transients a peak current occurs, which is higher than the steady-state short circuit current of 10 kA. In the worst case this peak short circuit current equals twice the steady-state short circuit current [9]. Therefore, for the transient AC calculations a single-phase short circuit current of 20 kA has been assumed as an upward estimate.

Regarding the parameters of the DC voltages and currents, all corresponding arrangements have been analyzed for a phase-to-phase voltage of ±10 kV and a line current of 0.5 kA during normal operation. For the transient analysis of fault conditions for the DC arrangements a single-phase fault current of 27 kA is considered. This is due to the assumption that the DC grid is fed by an AC grid with a short circuit current of maximum 20 kA at the converter's terminal. Further the usage of VSC-converters is assumed, therefore a maximum short circuit current at the AC side $I_{sc,ac}$ leads to a maximum short circuit current at the DC side of $I_{sc,dc} = \frac{3 \cdot \sqrt{2}}{\pi} \cdot I_{sc,ac}$ for the worst-case, a line-to-line short circuit in the DC grid.

All before mentioned voltages and currents have been modeled using ideal voltage and current sources. For the transient calculations, the above mentioned values of voltage and current are reached by ramping up from initial zero to the desired value. The ramp-up time for normal AC operating conditions is chosen as 60 ms, which corresponds to three periods of the AC fundamental frequency (50 Hz). For normal DC operating conditions it is assumed that the converters implement a ramp-up time of 60 ms. For fault conditions, the ramp-up time for AC is chosen as 10 ms, while for DC faults a faster ramp-up time of 5 ms is used due to the more dynamic behavior of DC grids compared to AC grids [10].

For every analyzed arrangement six calculations are performed. Firstly, normal operation conditions are considered. Therefore three calculations are performed, one with at both ends isolated influenced conductors, one with one side grounded and one with both sides grounded.

By doing so, the results show the range in which the voltages and currents for a real arrangement with a boundary network at the ends of the influenced conductors lay. Secondly, fault conditions are considered, again with three calculations for isolation at both ends, for one side grounded and for both sides grounded.

For the analysis under fault conditions, a single-phase fault is assumed. The phase which carries the fault current has always been selected as the phase, which is closest to the influenced conductors. An exception has been made if this phase would be the neutral conductor in a bipolar DC circuit. When considering one phase as fault afflicted, carrying the fault current, all other phases are considered to be in normal operation conditions. The voltages of the faulted phases are equal to the values during normal operation. Table 8 shows the fault afflicted phase regarding the considered arrangements.

Arrangement	Fault afflicted phase
AC overhead line – overhead line	W
DC overhead line – overhead line	N
AC overhead line – cable	W
DC overhead line – cable	N
AC cable – overhead line	V
DC cable – overhead line	P
AC cable – cable	W
DC cable – cable	N

Table 8: Fault afflicted phases in the considered arrangements

3.3 Results of Steady-state and Transient Analysis

First, the results of the steady-state analysis are presented. After that, the results of the transient analysis are presented. Finally, both, as far as practicable, are compared to show the coincidence between the results.

3.3.1 Steady-state Results

As shown in the analysis for steady-state EMI calculations only the interference caused by AC conductors needs to be considered. Therefore only the arrangements where the AC conductors cause the interference are examined. Table 9 shows the examined arrangements and their chronological order in this section. First, the results for normal operating conditions are shown. Afterwards the results for fault conditions are outlined.

Examined arrangements in chronological order
AC overhead line – overhead line
AC overhead line – cable
AC cable – overhead line
AC cable – cable

Table 9: Examined arrangements for steady state EMI

Normal operating conditions

Figure 12 shows the coupled line-to-earth RMS voltages on the conductors I_1, I_2 and I_3 due to EMI in normal operating conditions for the first arrangement. The coupled phase RMS currents are shown in Figure 13. It can be seen that the highest voltages appear for both sides being isolated. In this case, the RMS line-to-earth voltage on conductor I_1 reaches a maximum of 1870 V. The maximum voltages for one side grounded (30 V) and both sides grounded (15 V) are substantially lower. The highest currents appear if both sides are grounded. For both sides grounded the RMS phase current on conductor I_1 reaches a maximum of 25.2 A. If both sides are isolated (4 mA) or only one side is grounded (10 mA) the currents are significantly lower.

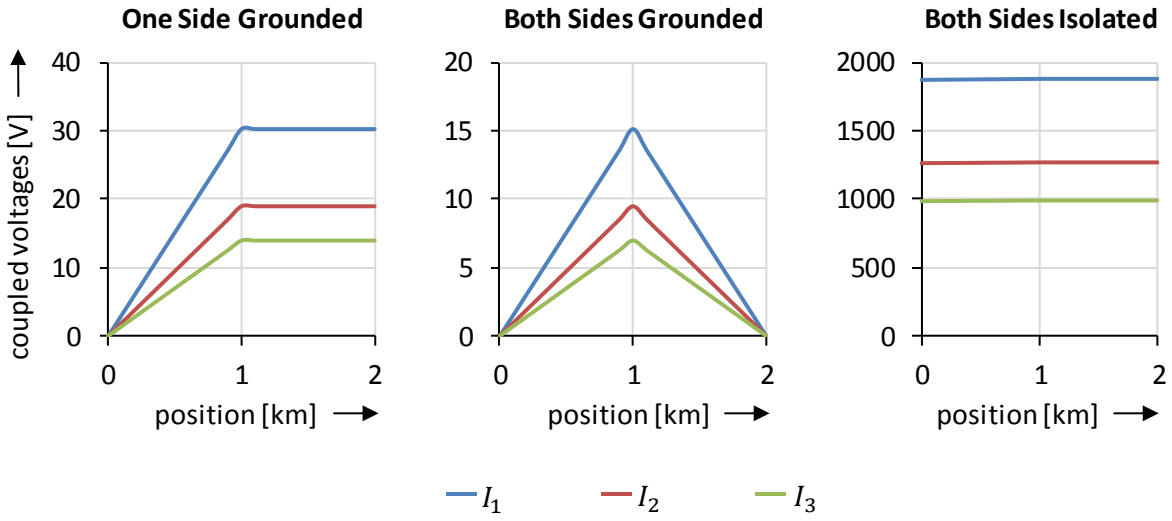

Figure 12: Coupled voltages in normal operating conditions (AC overhead line – overhead line)

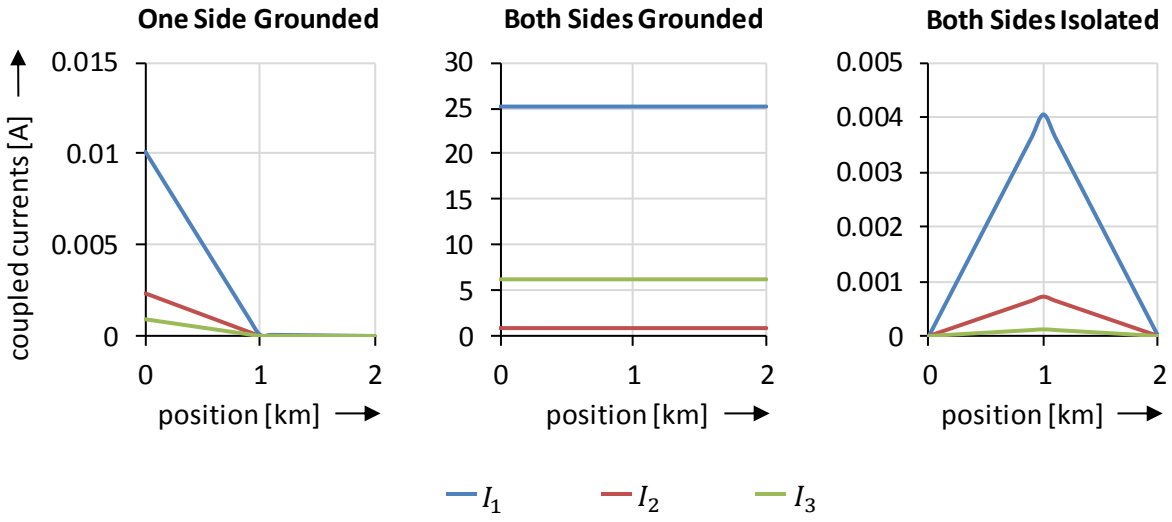

Figure 13: Coupled currents in normal operating conditions (AC overhead line – overhead line)

Figure 14 shows the coupled RMS line-to-earth voltages on the conductors I_1, I_2 and I_3 due to EMI in normal operating conditions for the second arrangement. The coupled RMS phase currents are shown in Figure 15. It can be seen that the highest voltages appear for one side grounded. In this case, the RMS line-to-earth voltage on conductor I_3 reaches a maximum of 1.6 mV. The maximum voltages for both sides isolated (1.2 mV) and both sides grounded (0.8 mV) are slightly lower. The highest RMS phase currents appear if both sides are grounded.

For both sides grounded the current on conductor I_3 reaches a maximum of 8.7 mA. If both sides are isolated (18 nA) or only one side is grounded (94 nA) the currents are significantly lower.

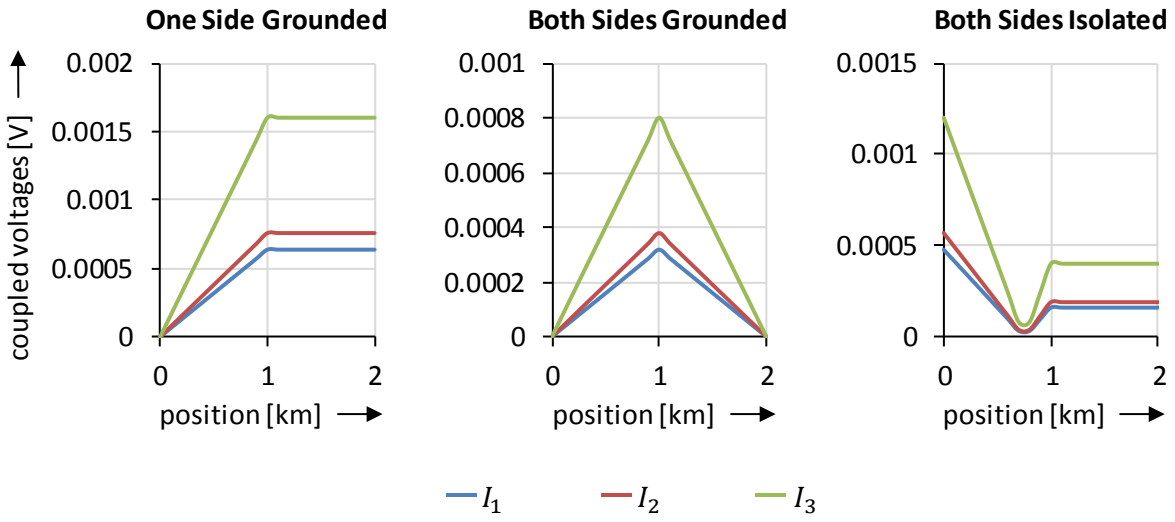

Figure 14: Coupled voltages in normal operating conditions (AC overhead line – cable)

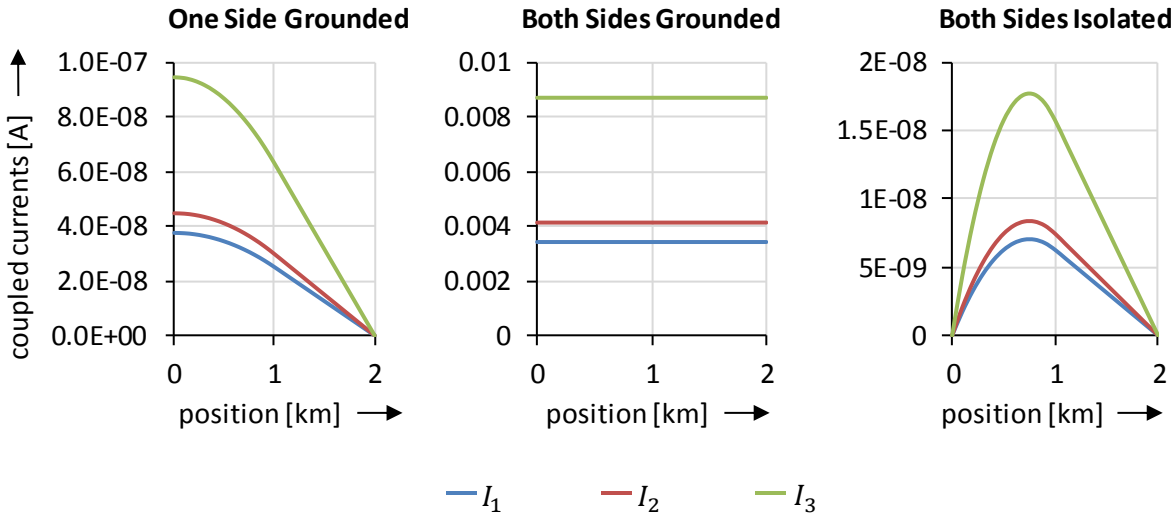

Figure 15: Coupled currents in normal operating conditions (AC overhead line – cable)

The coupled RMS line-to-earth voltages and the coupled RMS phase currents for the two other examined arrangements are similar to the shown curves for the second arrangement (AC overhead line – cable). Only the absolute height of the coupled voltages and currents differs. Therefore these values are summarized and described in section 3.3.2.

Fault conditions

Figure 16 shows the coupled line-to-earth RMS voltages on the conductors I_1, I_2 and I_3 due to EMI in fault conditions for the first arrangement. The coupled phase RMS currents are shown in Figure 17. It can be seen that the highest voltages appear if one side is grounded. In this case, the RMS line-to-earth voltage on conductor I_1 reaches a maximum of 4600 V. The maximum voltages for both sides grounded (2300 V) and both sides isolated (2950 V) are slightly lower. The highest currents appear if both sides are grounded. For both sides grounded the RMS phase current on conductor I_1 reaches a maximum of 2100 A. If both sides are isolated (5 mA) or only one side is grounded (14 mA) the currents are significantly lower.

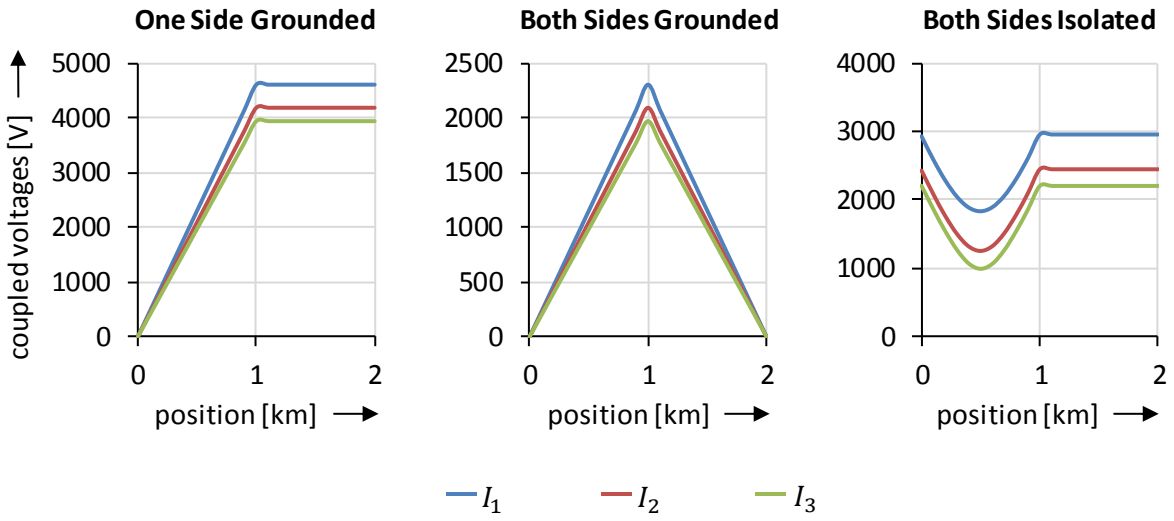

Figure 16: Coupled voltages in fault conditions (AC overhead line – overhead line)

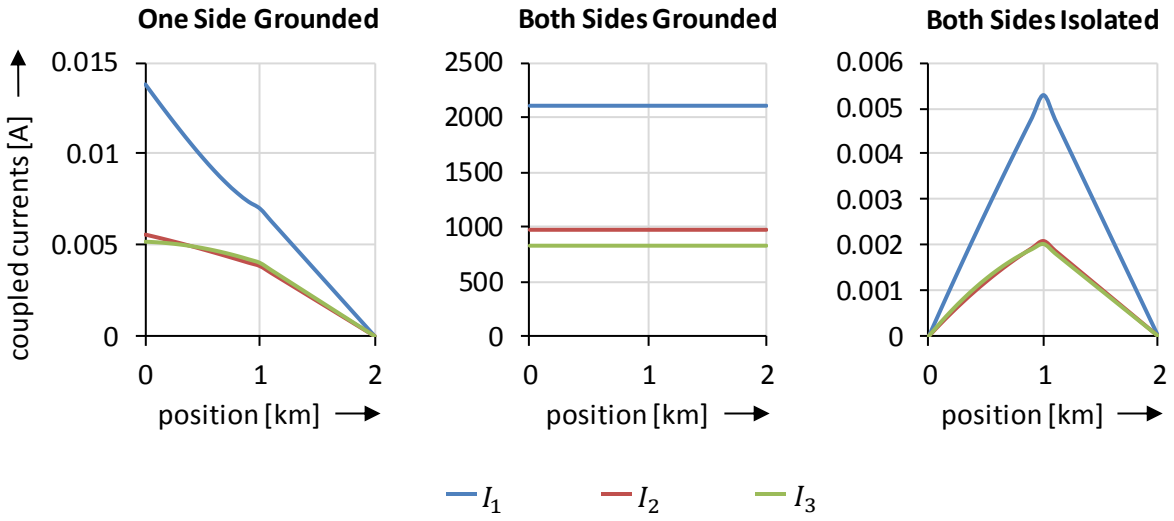

Figure 17: Coupled currents in fault conditions (AC overhead line – overhead line)

Figure 18 shows the coupled RMS line-to-earth voltages on the conductors I_1, I_2 and I_3 due to EMI in fault conditions for the second arrangement. The coupled RMS phase currents are shown in Figure 19. It can be seen that the highest voltages appear for one side grounded. In this case, the RMS line-to-earth voltage on conductor I_3 reaches a maximum of 13 V. The maximum voltages for both sides isolated (9.6 V) and both sides grounded (6.5 V) are slightly lower. The highest RMS phase currents appear if both sides are grounded. For both sides grounded the current on conductor I_2 reaches a maximum of 70 A. If both sides are isolated (0.144 mA) or only one side is grounded (0.75 mA) the currents are significantly lower.

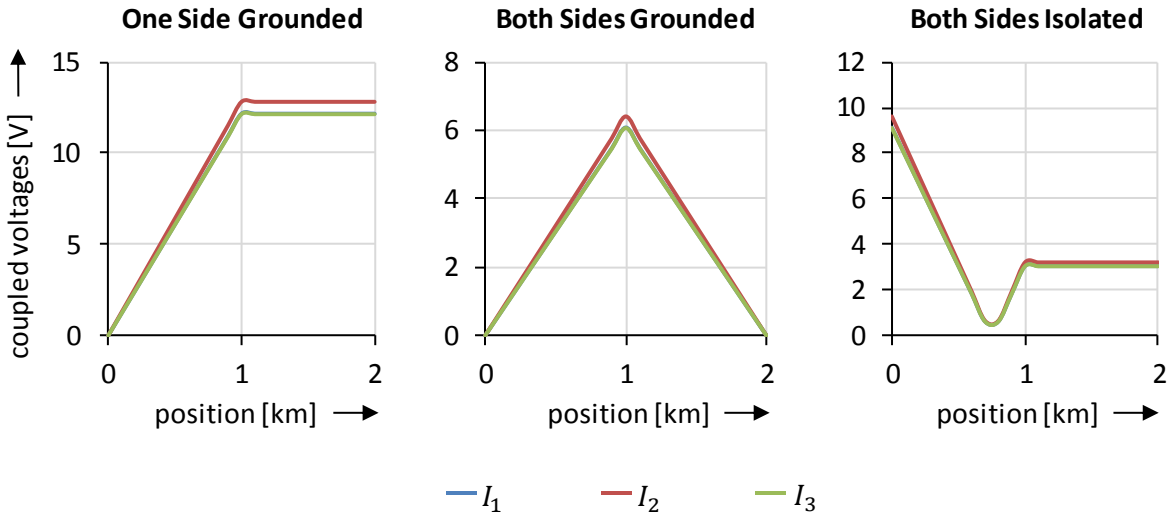

Figure 18: Coupled voltages in fault conditions (AC overhead line – cable)

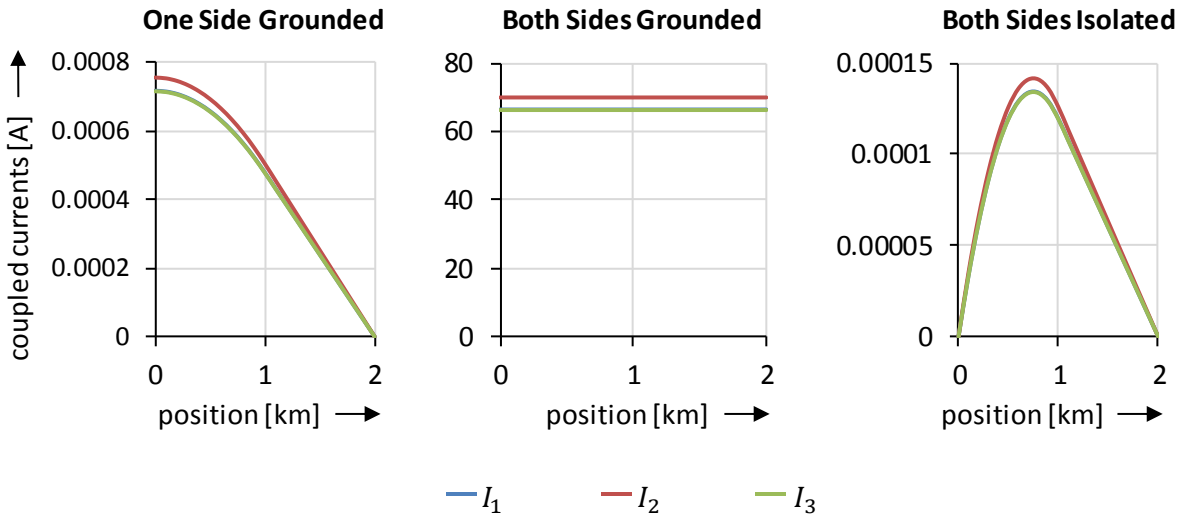

Figure 19: Coupled currents in fault conditions (AC overhead line – cable)

The coupled RMS line-to-earth voltages and the coupled RMS phase currents for the two other examined arrangements are similar to the shown curves for the second arrangement (AC overhead line – cable). Only the absolute height of the coupled voltages and currents differs. Therefore these values are summarized and described in the following section.

3.3.2 Summary of the Steady-state Results

Table 10 summarizes the results, which were partly presented in detail in the previous section. The maximum voltages and maximum currents are shown for both normal operating conditions and fault conditions for every examined arrangement. The results in the previous section showed that the maximum current always appears if both endpoints are grounded. The maximum voltage appears either if both or only one endpoint is isolated.

Arrangement	Normal operating conditions		Fault conditions	
	Max. voltage	Max. current	Max. voltage	Max. current
AC overhead line – overhead line	1870 V	25.2 A	4600 V	2100 A
AC overhead line – cable	1.6 mV	8.7 mA	13 V	70 A
AC cable – overhead line	35 mV	8.7 mA	13 V	4.8 A
AC cable – cable	37 mV	200 mA	1 V	5.3 A

Table 10: Maximum rms steady-state voltages and currents in normal operating conditions and fault conditions for AC

It can be seen that the highest mutual interference by far occurs between overhead lines. For this arrangement the maximum coupled voltage is 1870 V in normal operating conditions. During fault conditions the maximum voltage is even 4600 V and the maximum current rises from 25.2 A in normal operating conditions to 2100 A. The second highest mutual interference in normal operating conditions occurs between cables. In this case the maximum voltage reaches 37 mV and the maximum current 200 mA. The second highest mutual interference in fault conditions occurs for the “AC overhead line – cable” arrangement. The maximum voltage reaches 13 V and the maximum current 70 A. All other examined arrangements show even lower maximum voltages and maximum currents.

It is recommended to keep the steady-state fundamental component of the DC current ripple below 0.1% of the converter rating to ensure a negligible influence on the system's performance. Otherwise the effect on converter performance has to be studied [11]. This means, for a rated current of a converter of 500 A the coupled 50-Hz-current should not be higher than 500 mA. The presented results for the steady-state EMI show that for normal operating conditions only the EMI between overhead lines causes coupled 50-Hz-currents higher than 0.5 A. Therefore, for real networks the EMI between AC- and DC-systems in normal operating conditions has only to be considered for overhead lines. For fault conditions, the coupled 50-Hz-current is higher than 0.5 A for every examined arrangement. Nevertheless, it has also to be considered that this interference only occurs for the few seconds of fault conditions in the AC-System.

3.3.3 Transient Results for Arrangements with AC Conductors only

The already introduced steady-state results for AC conductors are validated by comparing them with the transient results for AC conductors. Therefore the transient results for normal operating conditions and for fault conditions are shown. Opposite to the steady-state results, for the transient results only the voltages and currents at the beginning, the middle and the end of the conductors are shown.

For every arrangement in normal operating conditions and fault conditions nine plots can be generated. In the following only the two plots with the maximum voltages and maximum currents for every arrangement are shown. For easier comparability of the transient results with the steady-state results in normal operation, the corresponding steady-state peak values are shown as horizontal lines in the following plots. For fault conditions, opposite to the previous steady-state calculations, the maximum possible peak short circuit current has been taken into account. In the worst case this current is equal twice the steady-state short circuit current and is therefore an upward estimate, as described already before. All maximum voltages and currents are summarized in section 3.3.4.

Due to the larger transient short circuit current, the transient results for fault conditions are not comparable with the before shown steady-state results. But by comparing the steady-state results with the transient results for normal operating conditions, it is already shown that both calculation methods yield the same results.

Normal operating conditions

Figure 20 and Figure 21 show the maximum coupled transient line-to-earth voltages and maximum coupled transient currents on the conductors I_1, I_2 and I_3 due to EMI in normal operating conditions for the first AC arrangement. The maximum coupled transient voltages occur for both sides isolated while the maximum coupled transient currents occur for both sides grounded. Compared to the corresponding steady-state results it can be seen that the steady-state and the transient results coincide after steady-state has been reached.

The transient results in normal operating conditions for the three other examined arrangements (AC overhead line – cable, AC cable – overhead line as well as AC cable - cable) coincide with the steady-state results after steady-state has been reached. Noteworthy is that for the fourth arrangement (AC cable – cable) with both sides isolated the transient voltages show a different behavior than in the arrangements before. As shown in Figure 22, before steady-state is reached, the maximum voltages are slightly larger than the steady-state peak values and more time is needed to reach the steady-state. This behavior is typical for cable-only arrangements [12].

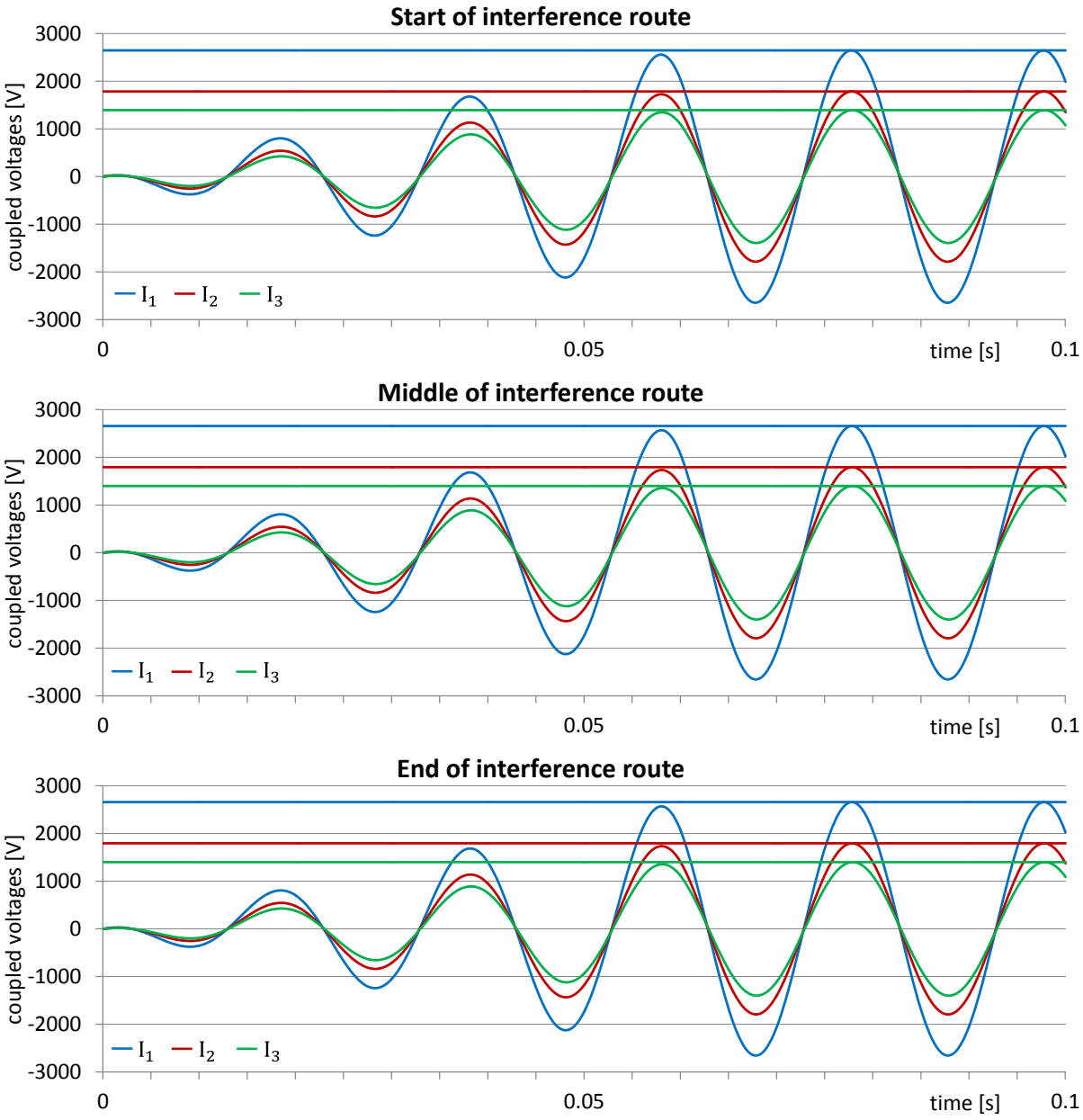

Figure 20: Coupled transient voltages in normal operating conditions (AC overhead line - overhead line) for both sides isolated

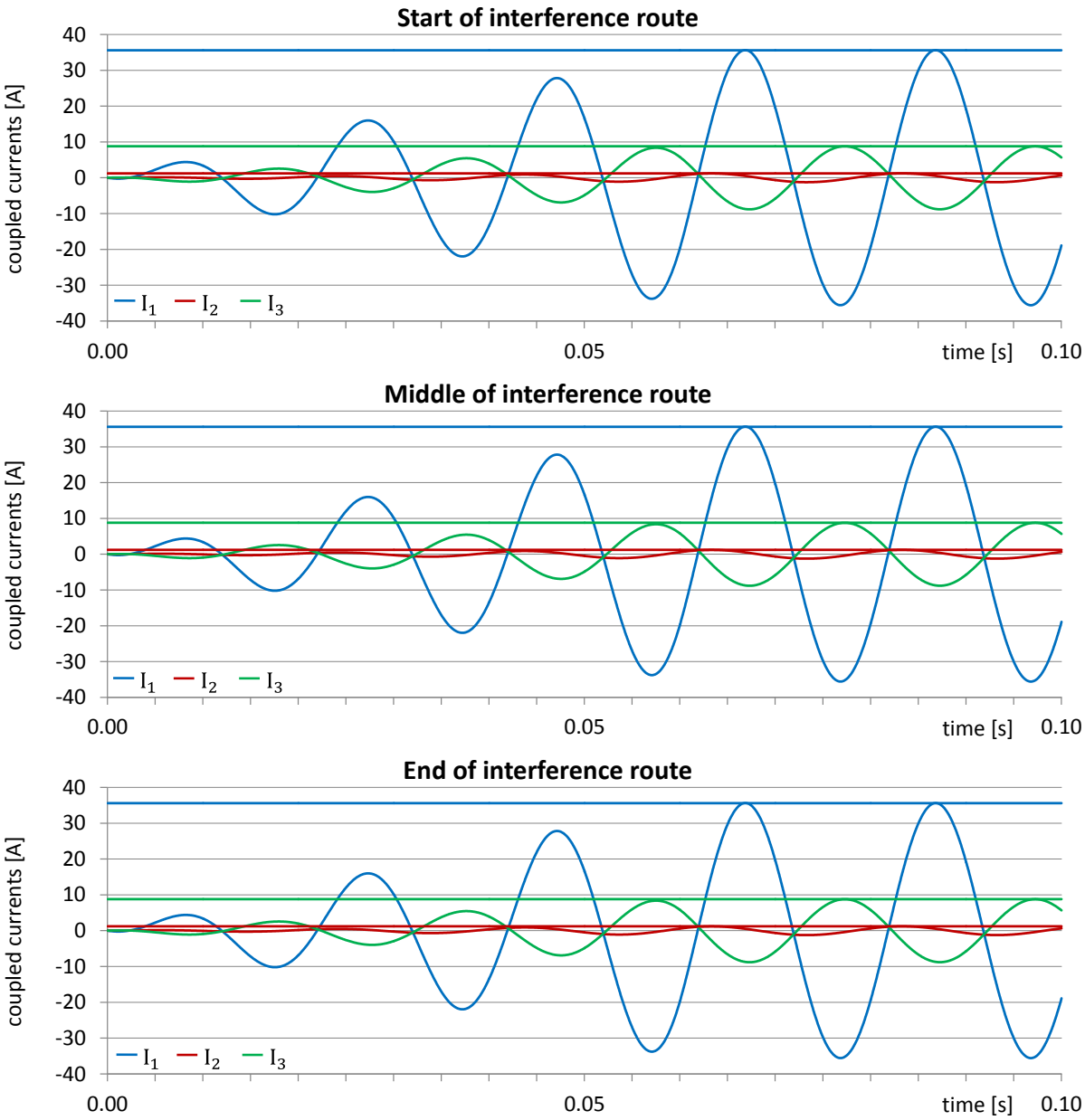

Figure 21: Coupled transient currents in normal operating conditions (AC overhead line - overhead line) for both sides grounded

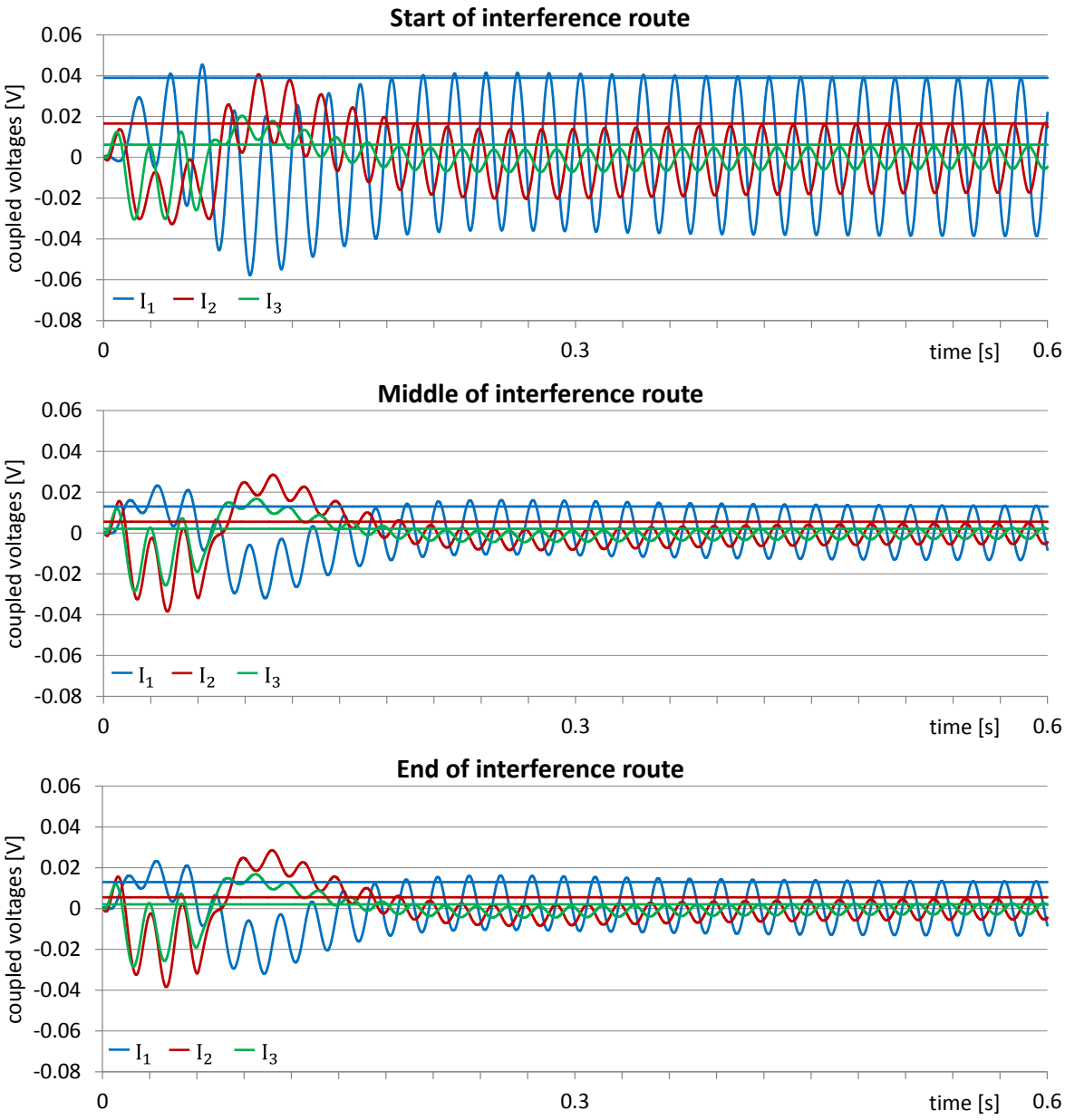

Figure 22: Coupled transient voltages in normal operating conditions (AC cable - cable) for both sides isolated

Fault conditions

Figure 23 and Figure 24 show the maximum coupled transient line-to-earth voltages and maximum coupled transient currents on the conductors I_1, I_2 and I_3 due to EMI in fault conditions for the first AC arrangement. The maximum coupled transient voltages occur for one side grounded (13.3 kV) while the maximum coupled transient currents occur for both sides grounded (6.1 kA). The maximum voltages for both sides isolated and both sides grounded are substantially lower, for both sides isolated or only one side grounded, the maximum currents are significantly lower.

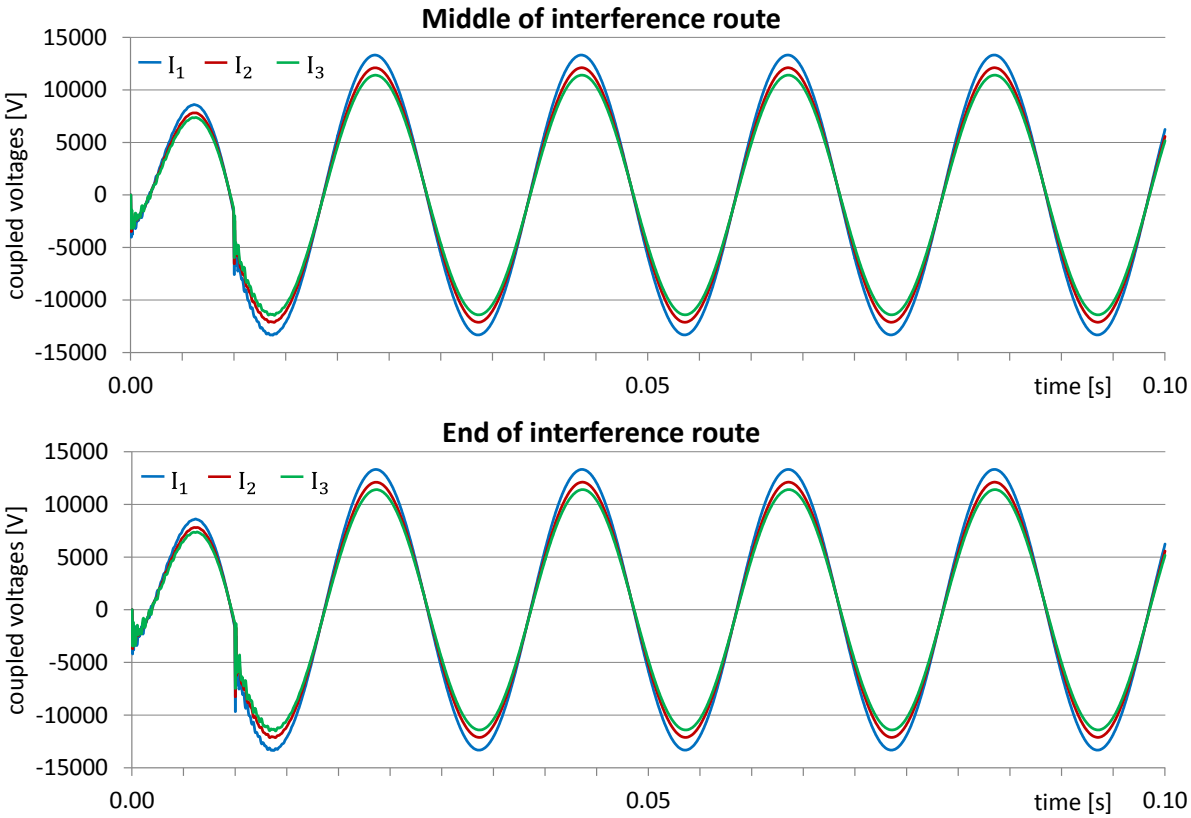

Figure 23: Coupled transient voltages in fault conditions (AC overhead line - overhead line) for one side grounded

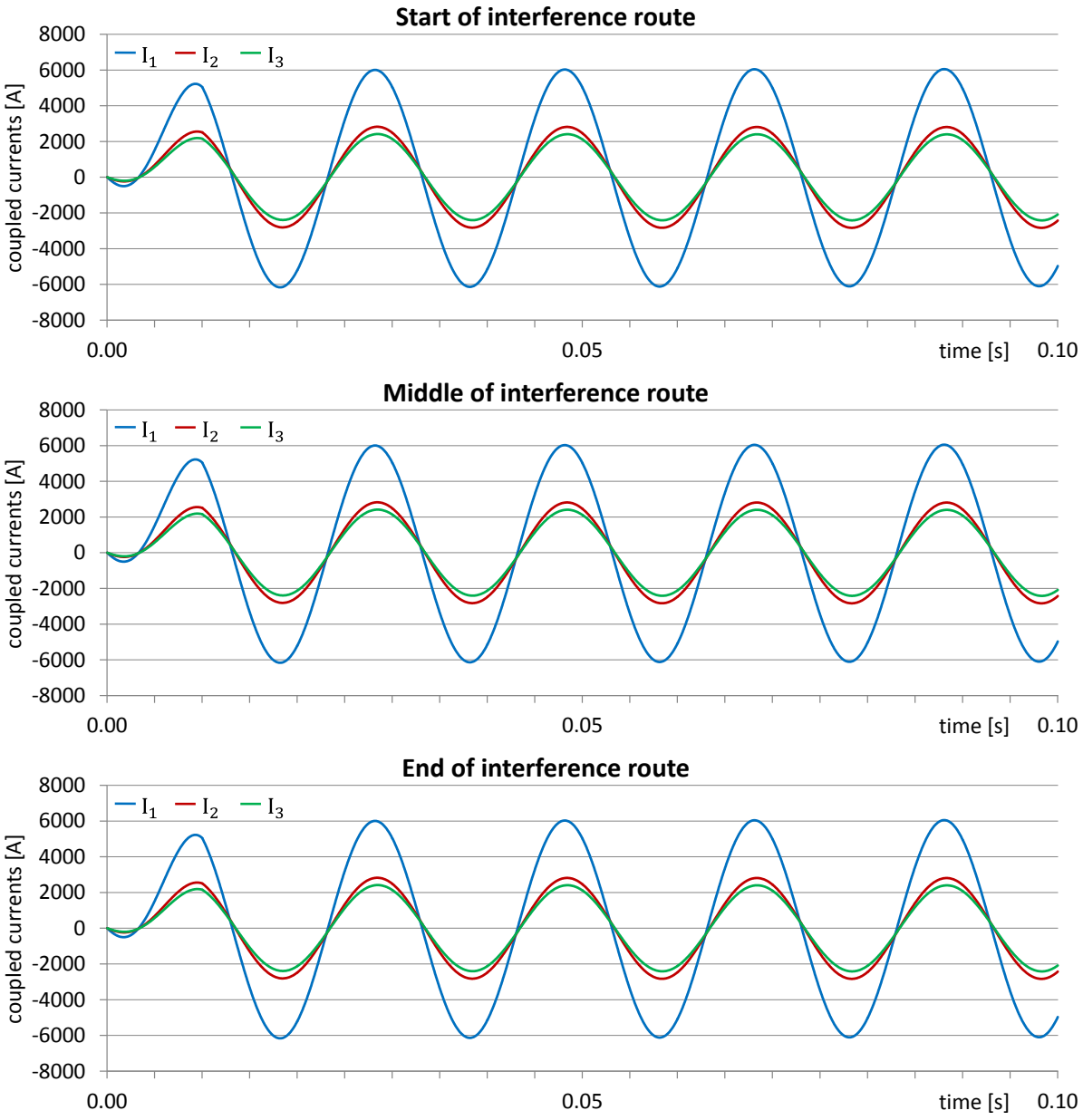

Figure 24: Coupled transient currents in fault conditions (AC overhead line - overhead line) for both sides grounded

The transient results in fault conditions for the other examined arrangements (AC overhead line – cable, AC cable – overhead line as well as AC cable - cable) are similar to the shown curves for the first arrangement. Noteworthy is that for the third arrangement (AC cable – overhead line) with both sides grounded the transient currents show a different behavior than in the arrangements before. As shown in Figure 25, before steady-state is reached, the maximum currents are larger (21 A) than the maximum steady-state peak values (14 A). The same holds

true for the fourth arrangement (AC cable – cable). The transient voltages for one side grounded, as shown in Figure 26, reach a maximum value of 3.7 V before the steady-state with a peak value of maximum 2.8 V is reached. The transient currents for both sides grounded, as shown in Figure 27, reach a maximum value of 30 A before the steady-state with a peak value of maximum 15.3 A is reached.

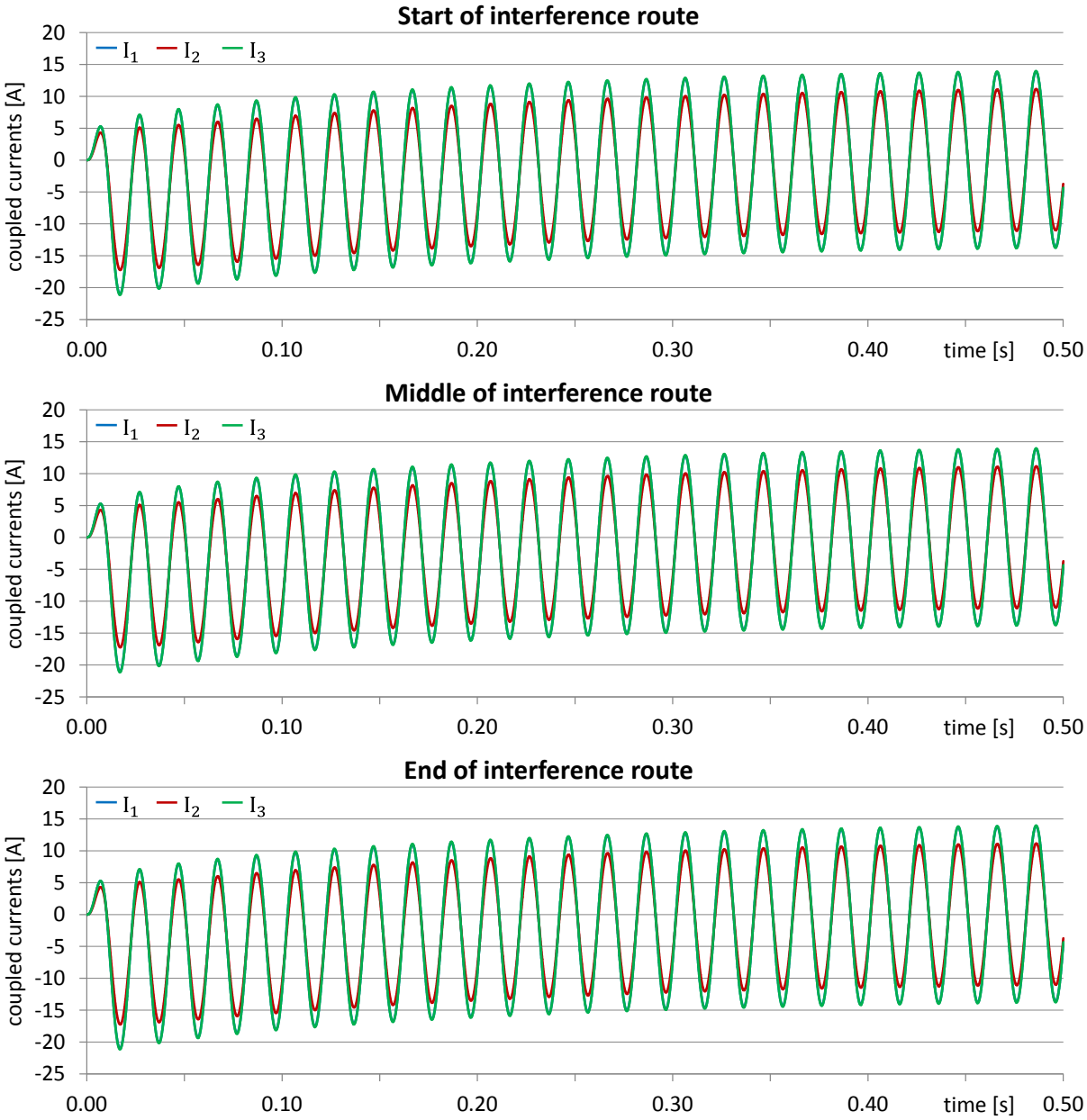

Figure 25: Coupled transient currents in fault conditions (AC cable - overhead line) for both sides grounded

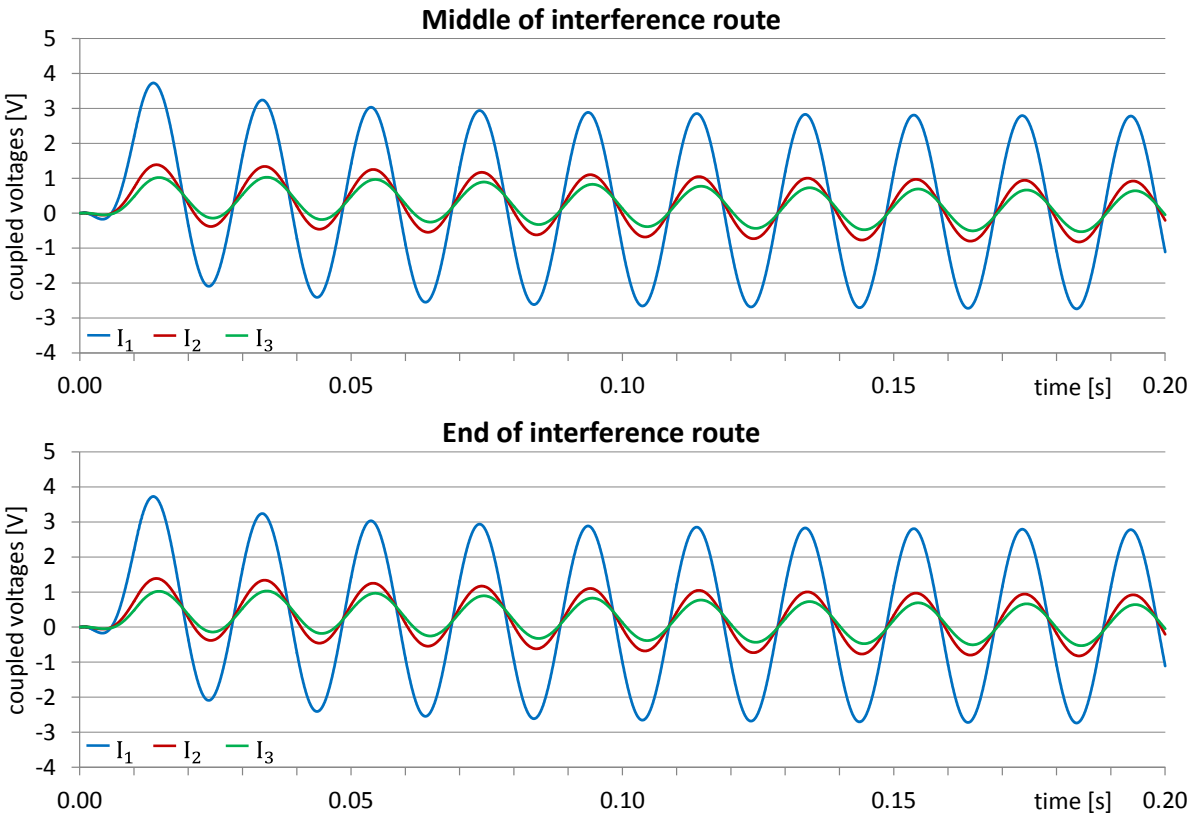

Figure 26: Coupled transient voltages in fault conditions (AC cable - cable) for one side grounded

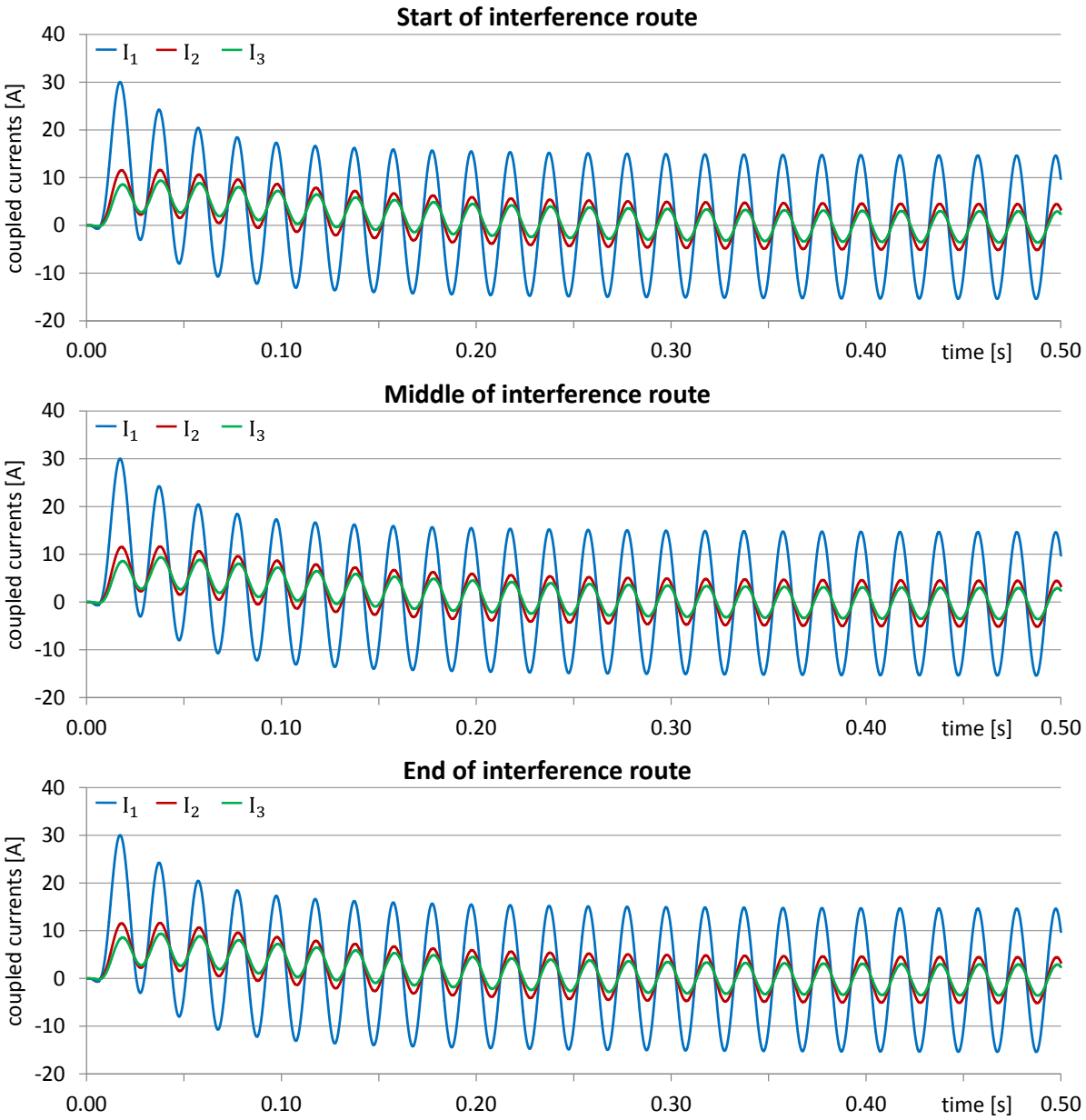

Figure 27: Coupled transient currents in fault conditions (AC cable - cable) for both sides grounded

3.3.4 Summary of Transient Results for AC

Table 11 summarizes the transient AC results, which were presented in more detail in the previous section. The maximum coupled transient voltages and maximum coupled transient currents for both normal operating conditions and fault conditions for every examined arrangement are shown. It has to be noted that for fault conditions, by using the peak short circuit current instead of the steady-state short circuit current, an upward estimate has been calculated. Therefore, compared to the steady-state results in Table 10, the maximum voltages and currents for fault conditions do not coincide and are much larger. Different from the steady-state results for normal operating conditions is the maximum voltage for the arrangement AC cable – cable due to the transient behavior of cables. Nevertheless, compared to the steady-state results (37 mV), the coupled voltage is still very small with its maximum at 56 mV.

Arrangement	Normal operating conditions		Fault conditions	
	Max. voltage	Max. current	Max. voltage	Max. current
AC overhead line – overhead line	1870 V rms	25.2 A rms	13.3 kV peak	6.1 kA peak
AC overhead line – cable	1.6 mV rms	8.7 mA rms	37 V peak	215 A peak
AC cable – overhead line	35 mV rms	8.7 mA rms	37 V peak	21 A peak
AC cable – cable	56 mV peak	200 mA rms	3.7 V peak	30 A peak

Table 11: Maximum transient rms and peak voltages and currents in normal operating conditions and fault conditions for AC

3.3.5 Transient Results for Arrangements with DC Conductors only

In the following the transient results for arrangements with DC conductors in normal operating conditions and for fault conditions are presented. Only the voltages and currents at the beginning, the middle and the end of the influenced conductors are shown. Table 12 shows the examined arrangements and their chronological order in this section. First, the results for normal operating conditions are shown. Afterwards the results for fault conditions are shown. All maximum voltages and currents are summarized in section 3.3.6.

Examined arrangements in chronological order
DC overhead line – overhead line
DC overhead line – cable
DC cable – overhead line
DC cable – cable

Table 12: Examined DC arrangements for transient EMI

For every arrangement in normal operating conditions and fault conditions nine plots are possible. In the following only two plots with the maximum voltages and maximum currents for every arrangement are shown. Every plot shows only the most interesting part of the transient voltages and currents. All voltages and currents decay to zero, even if not shown in the plot.

Normal operating conditions

Figure 28 and Figure 29 show the coupled transient line-to-earth voltages and coupled transient currents on the conductors I_1, I_2 and I_3 due to EMI in normal operating conditions for the first DC arrangement from Table 12. The maximum coupled transient voltages appear for both sides isolated. In this case, the transient line-to-earth voltage on conductor I_1 reaches a maximum of 1650 V. The maximum voltages for one side grounded and both sides grounded are substantially lower. The maximum coupled transient currents appear for both sides grounded. In this case, the transient phase current on conductor I_1 reaches a maximum of 18 A. If both sides are isolated or only one side is grounded, the maximum currents are significantly lower.

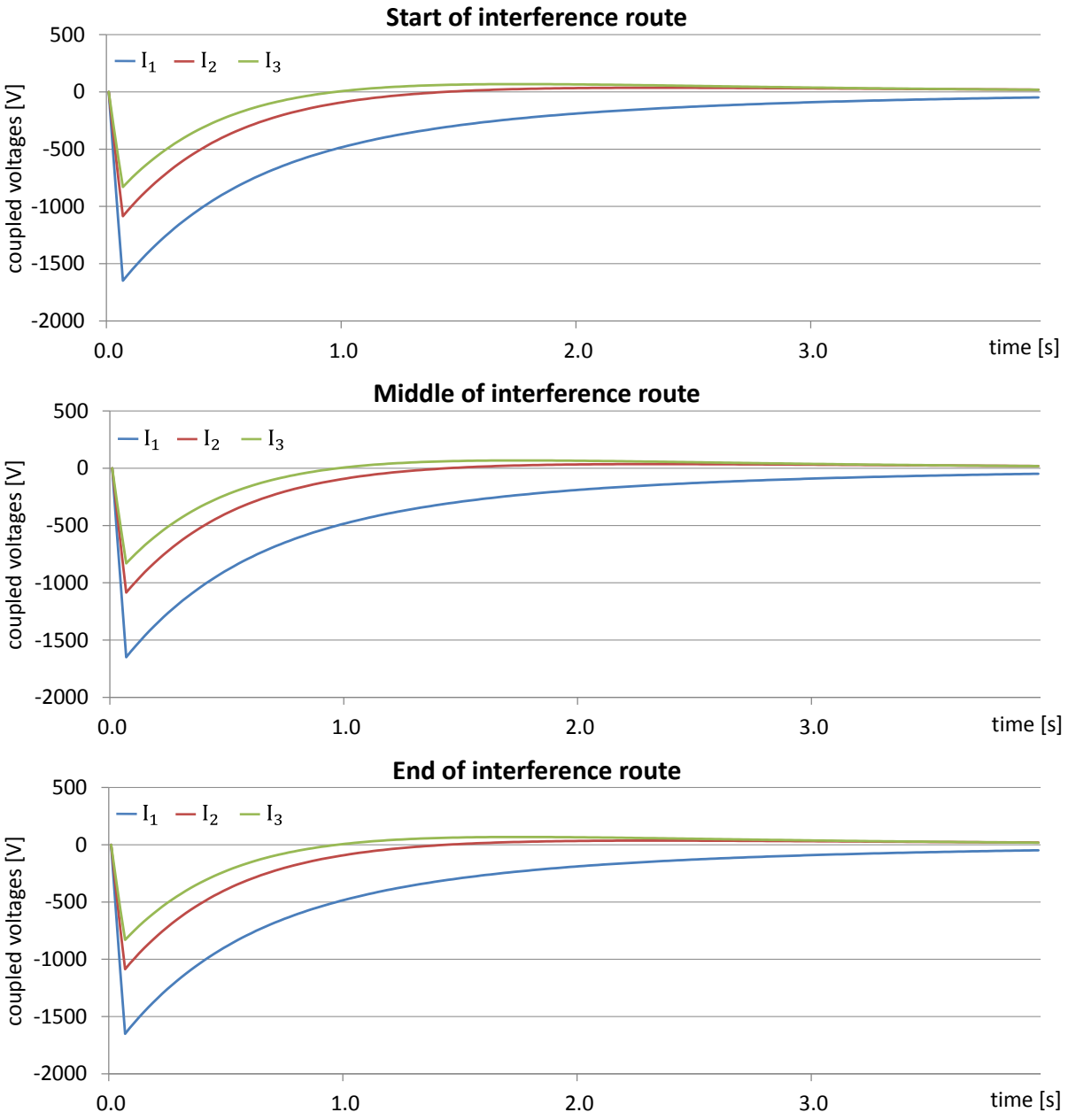

Figure 28: Coupled transient voltages in normal operating conditions (DC overhead line – overhead line) for both sides isolated

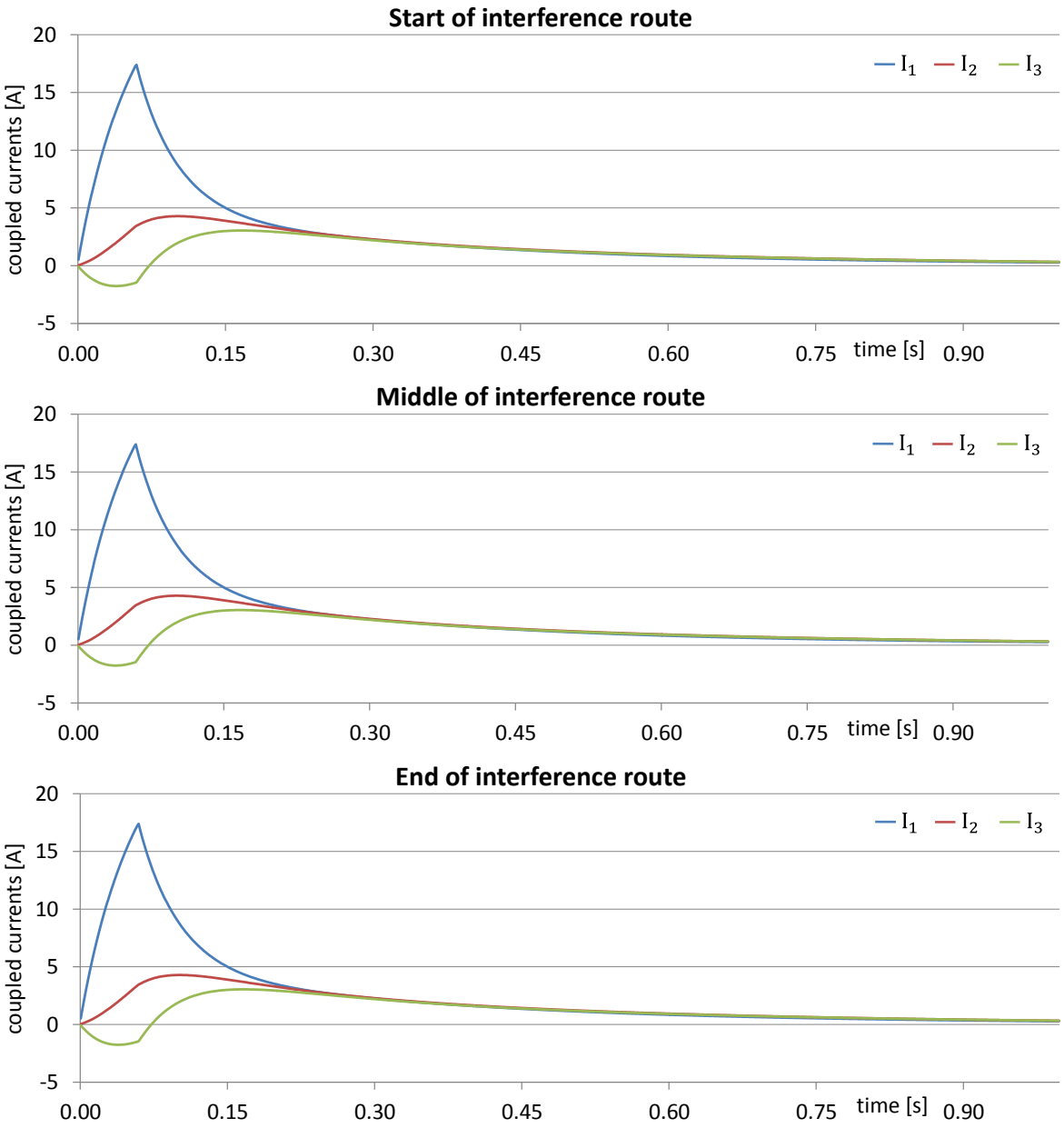

Figure 29: Coupled transient currents in normal operating conditions (DC overhead line – overhead line) for both sides grounded

The transient results in normal operating conditions for the two other examined arrangements (DC overhead line – cable, DC cable – overhead line) are similar to the shown curves of the first arrangement, but with much lower maximum voltages and currents. For the fourth arrangement (DC cable – cable) the curves look different and have larger values, as shown for the maximum voltages in Figure 30 and for the maximum currents in Figure 31.

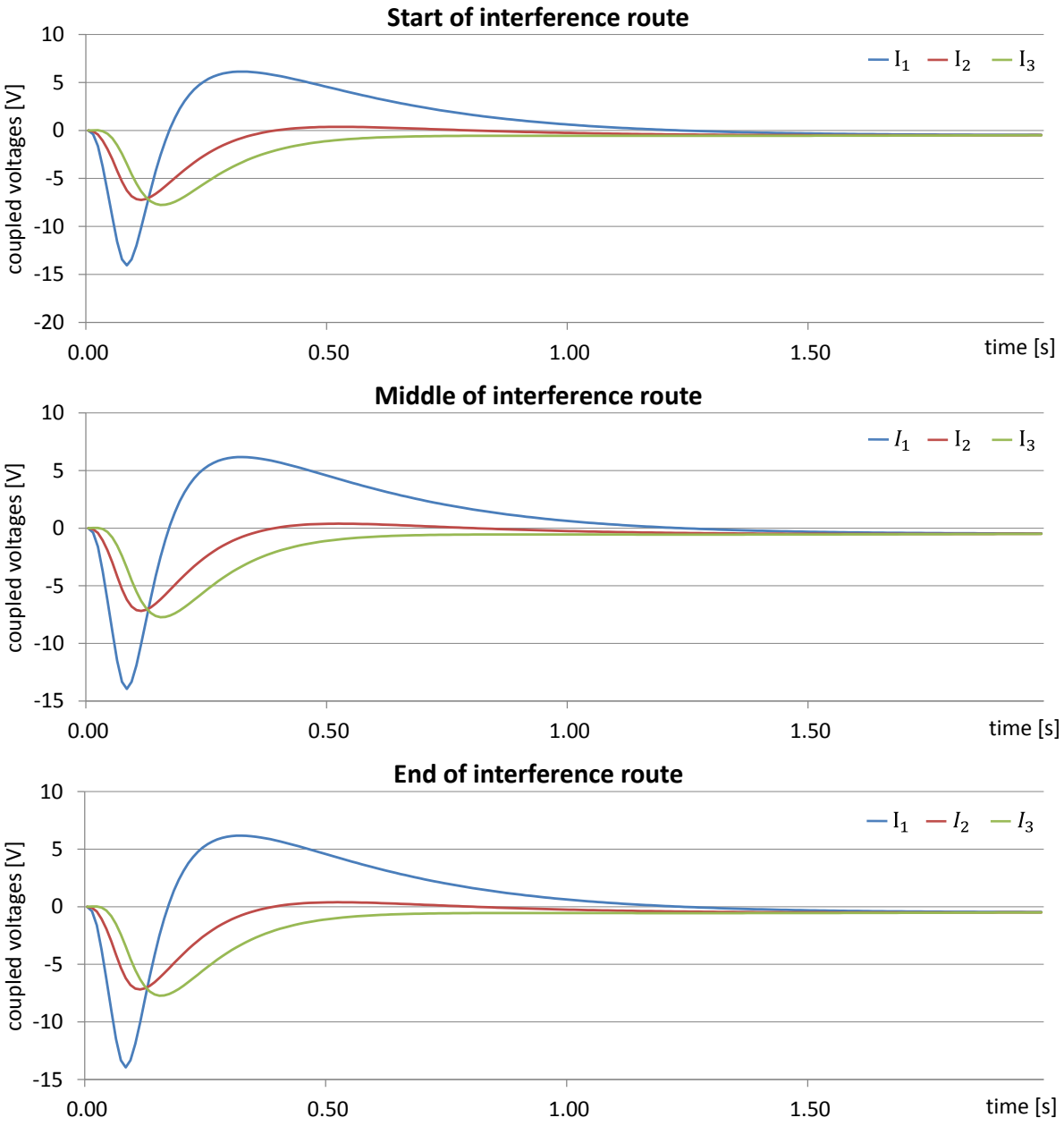

Figure 30: Coupled transient voltages in normal operating conditions (DC cable - cable) for both sides isolated

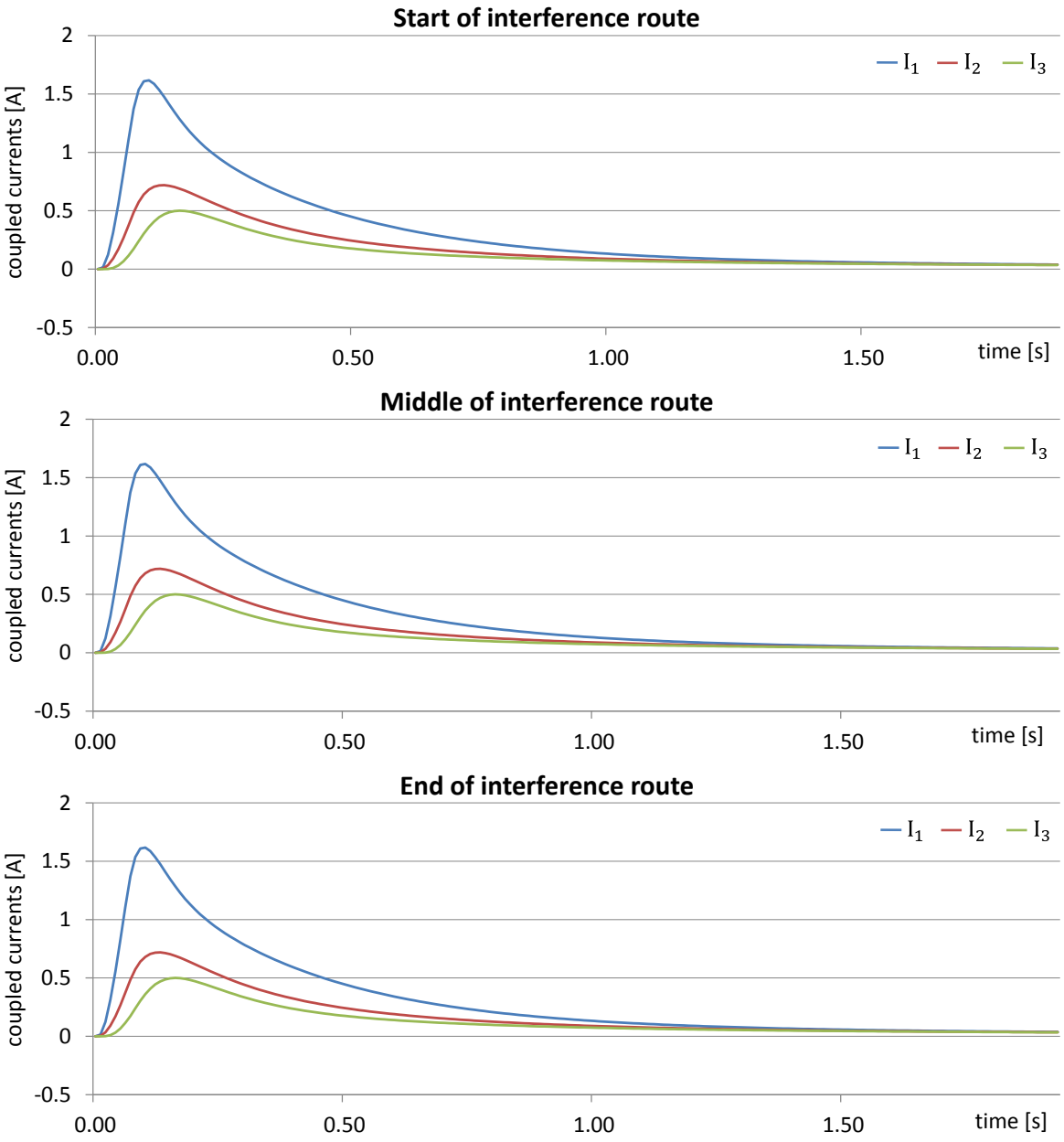

Figure 31: Coupled transient currents in normal operating conditions (DC cable - cable) for both sides grounded

Fault conditions

Figure 32 and Figure 33 show the coupled transient line-to-earth voltages and coupled transient currents on the conductors I_1, I_2 and I_3 due to EMI in fault conditions for the first DC arrangement from Table 12. The maximum coupled transient voltages appear for both sides isolated. In this case, the transient line-to-earth voltage on conductor I_1 reaches a maximum of 6026 V. The maximum voltages for one side grounded and both sides grounded are substantially lower. The maximum coupled transient currents appear for both sides grounded. In this case, the transient phase current on conductor I_1 reaches a maximum of 2608 A. If both sides are isolated or only one side is grounded, the maximum currents are significantly lower.

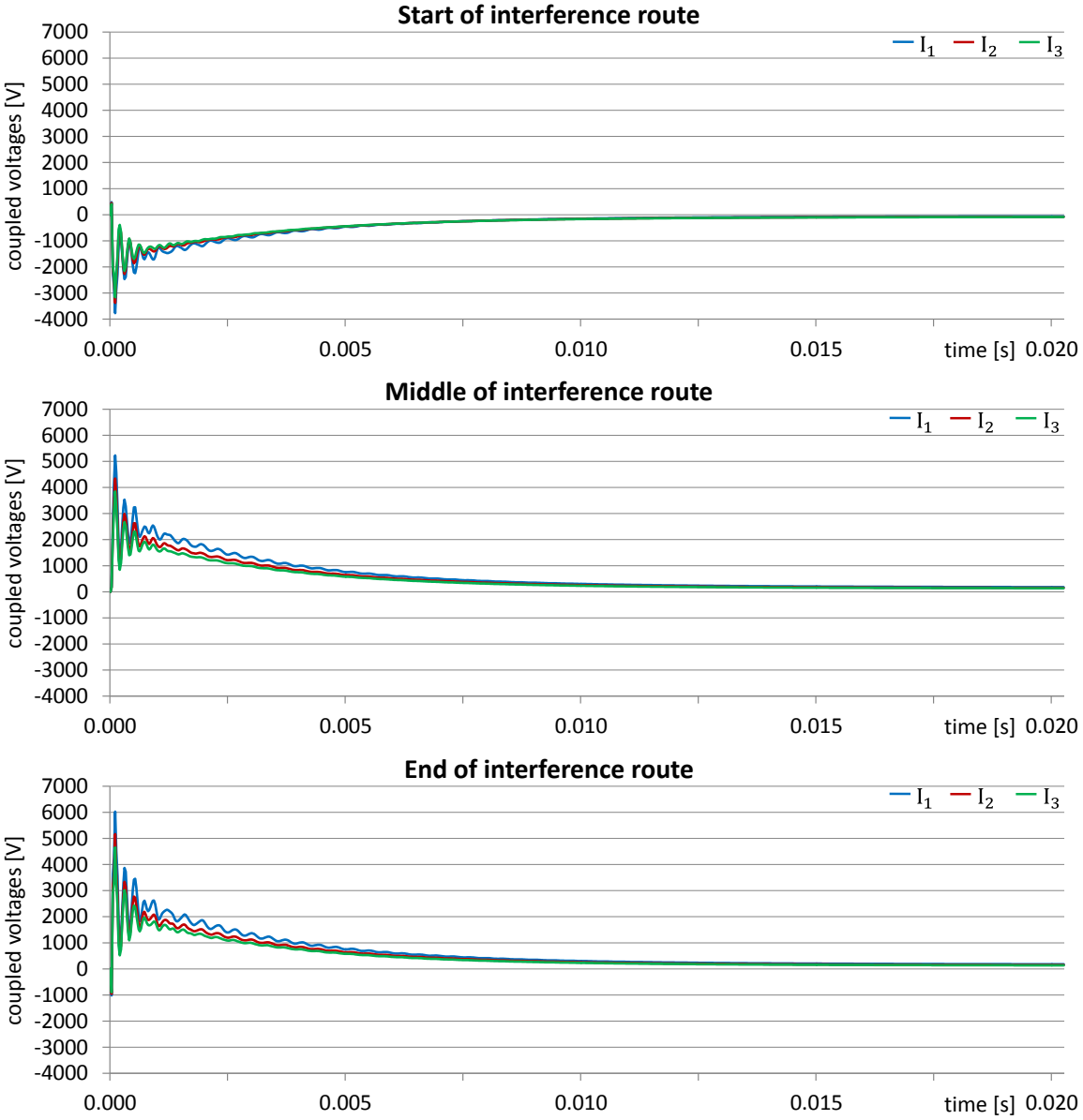

Figure 32: Coupled transient voltages in fault conditions (DC overhead line - overhead line) for both sides isolated

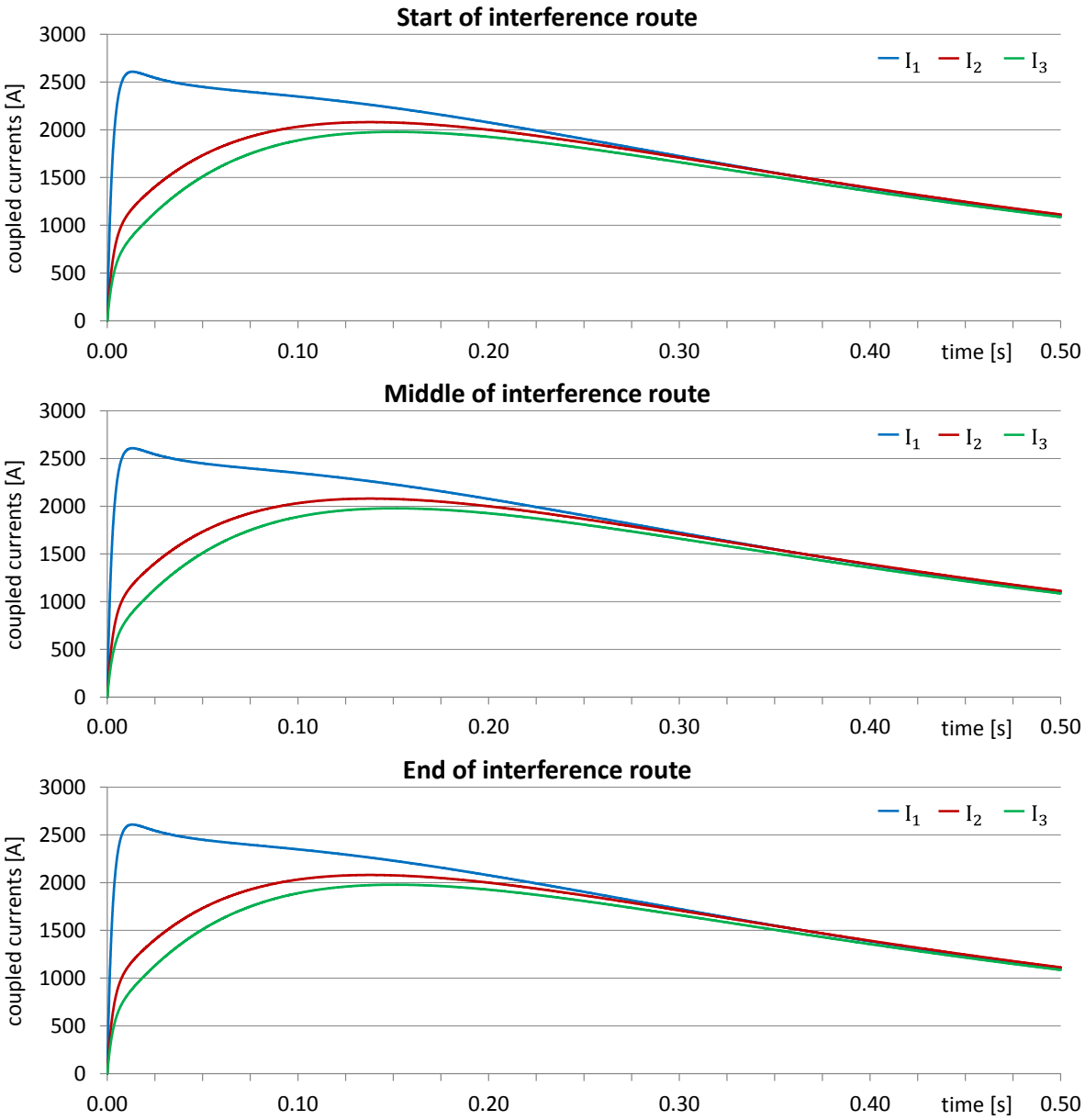

Figure 33: Coupled transient currents in fault conditions (DC overhead line - overhead line) for both sides grounded

Figure 34 and Figure 35 show the coupled transient line-to-earth voltages and coupled transient currents on the conductors I_1, I_2 and I_3 due to EMI in fault conditions for the second DC arrangement from Table 12. The maximum coupled transient voltages appear for one side grounded. In this case, the transient line-to-earth voltages on all three conductors reach a maximum of 31 V. The maximum voltages for both sides isolated and both sides grounded are substantially lower. The maximum coupled transient currents appear for both sides grounded. In this case, the transient phase current on all three conductors reach a maximum of 488 A.

If both sides are isolated or only one side is grounded, the maximum currents are significantly lower.

The transient results in fault conditions for the two other examined arrangements (DC cable - overhead line, DC cable – cable) are similar to the shown curves of the first and second arrangement.

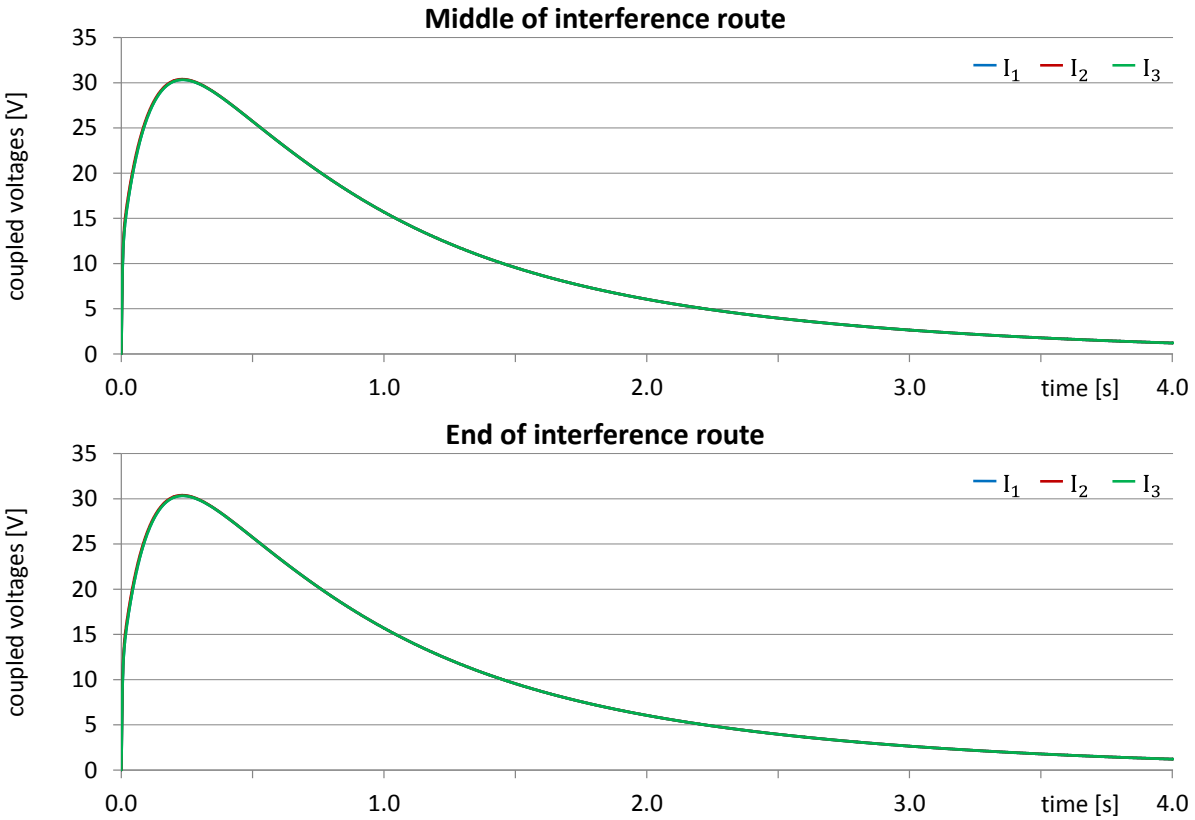

Figure 34: Coupled transient voltages in fault conditions (DC overhead line - cable) for one side grounded

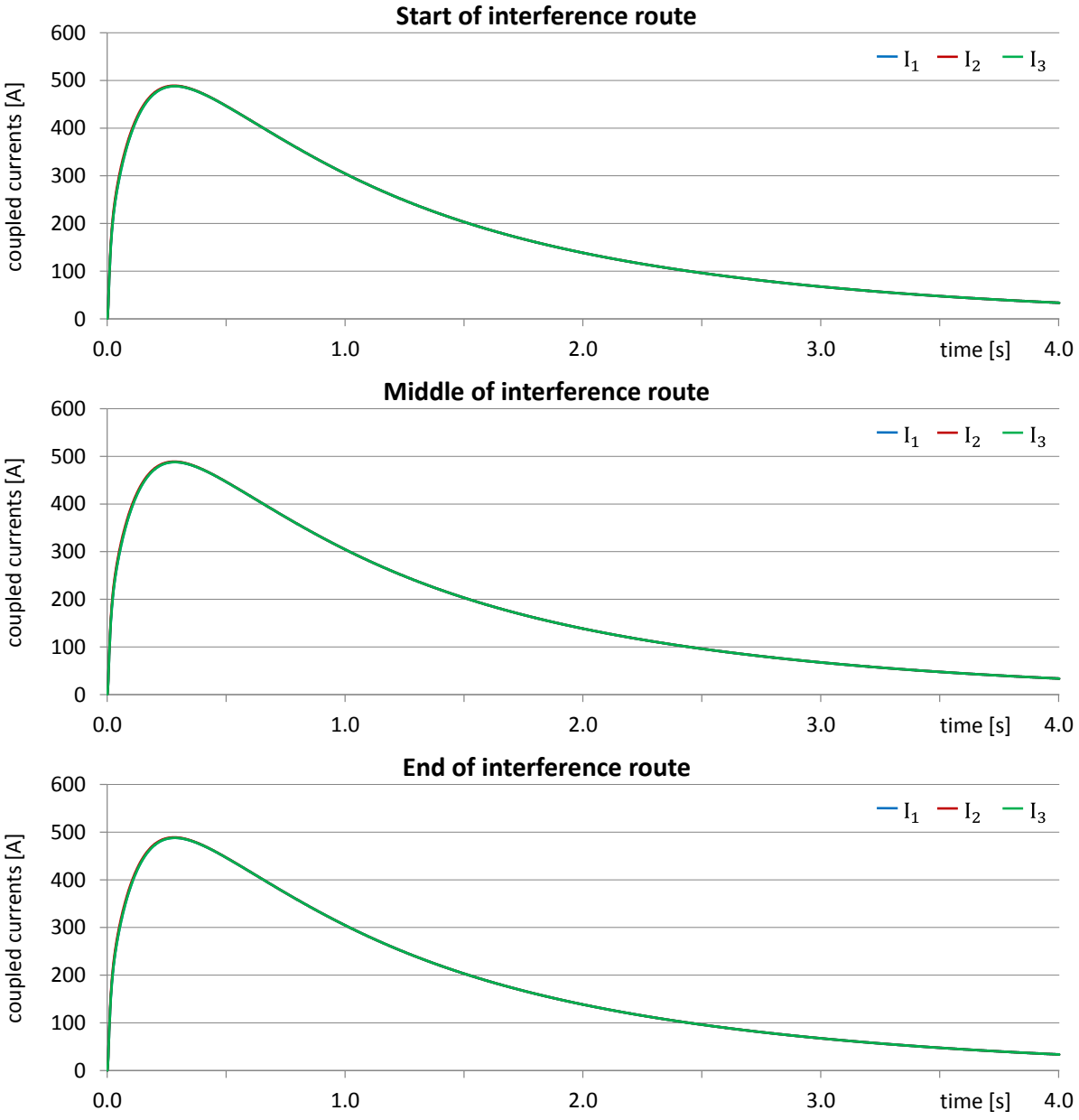

Figure 35: Coupled transient currents in fault conditions (DC overhead line - cable) for both sides grounded

3.3.6 Summary of Transient Results for DC

Table 13 summarizes the transient DC results, which were presented in more detail in the previous section. The maximum voltages and maximum currents for both normal operating conditions and fault conditions for every examined arrangement are shown.

Arrangement	Normal operating conditions		Fault conditions	
	Max. voltage	Max. current	Max. voltage	Max. current
DC overhead line – overhead line	1650 V	18 A	6026 V	2608 A
DC overhead line – cable	1.1 mV	17 mA	31 V	488 A
DC cable – overhead line	1.8 mV	15 mA	38 V	561 A
DC cable – cable	14 V	1.6 A	19 V	318 A

Table 13: Maximum transient peak voltages and currents in normal operating conditions and fault conditions for DC

It can be seen that the highest mutual interference by far occurs between overhead lines. For this arrangement the maximum coupled voltage is 1650 V in normal operating conditions. In fault conditions the maximum voltage is 6026 V and the maximum current rises from 18 A in normal operating conditions to 2608 A. All other examined arrangements show significantly lower maximum voltages and maximum currents in normal operating conditions. In fault conditions, also the other three arrangements show larger maximum voltages and currents than in normal operating conditions, ranging from 19 V up to 38 V and from 318 A up to 561 A, respectively. The results in the previous section showed that the maximum current always appears if both endpoints are grounded. The maximum voltage appears either if both or only one endpoint is isolated.

The transient results for DC overhead lines and cables show that in normal operating conditions as well as in fault conditions significant mutual coupling between multiple overhead lines occur. In fault conditions the mutual coupling between overhead lines and cables as well as between multiple cables is significant, too. Therefore it can be summarized that for every parallel operation of medium voltage DC overhead lines and/or cables with other overhead lines

and/or cables the transient mutual electromagnetic interference has to be investigated. The influence of such injected currents and induced voltages on other operating resources is pointed out in chapter 4.

4 Influence of Injected Currents and Induced Voltages on other Operating Resources

In conductors of neighboring circuits injected currents and induced voltages may have an influence on adjacent operating resources. Especially in fault conditions such injected currents and induced voltages may increase largely. The induced voltages can have a negative influence on the insulation of nearly every operating resource. The injected currents can have a negative influence on power and instrument transformers as well as converters. Due to the influence on instrument transformers, the grid's protection system, which relies on the instrument transformers, can also experience a negative influence. This may lead to false tripping or prolonged fault clearing times [13].

First, the effects of injected DC currents on power and instrument transformers are considered. After that, the effects of injected AC currents on converters are highlighted. Finally, some options to mitigate these effects are presented.

4.1 Power Transformers under DC Bias

Injected DC currents cause a DC bias in the magnetizing current of transformers. Those DC currents cause the transformer core to saturate during the half-cycle in which the bias current flows in the same direction as the magnetizing current. Consequently, some undesirable effects such as increased noise, excessive core vibrations and overheating occur. Such effects pose a potential threat for the integrity and longevity of the transformer. Furthermore, due to a DC bias a transformer becomes a harmonic source, which is harmful for the secure and stable operation of power systems [14].

4.1.1 Magnetic Core Saturation

One of the major effects of a DC bias is the tendency towards half-cycle (asymmetric) saturation [15]. The order of magnitude of the DC current necessary to saturate the transformer is the same as that of the transformer no-load current. These are usually few percent of the nominal current. When the magnetic circuit of the transformer is saturated, the relative permeability of its constituent material decreases significantly with the increase in the level of saturation of the magnetic circuit. As a result of the saturation, the magnetizing impedance of the transformer (and the relative permeability of the magnetic material) also decreases significantly [16]. The saturation of the transformer's magnetic core can also lead to long-term deterioration [11].

4.1.2 Generation of Harmonics

During the saturated half-cycle an increase in magnetizing current will be experienced. This will result in a non-linear current waveform, containing an assortment of odd and even harmonics [17]. This is a particularly undesirable condition, which is recognized in the IEEE standard "General Requirements for Liquid-Immersed Distribution, Power, and Regulating Transformers". It states that power transformers should not be expected to carry load currents with a harmonic factor greater than 5% of its rating [18]. Due to a DC bias, transformers become a significant source of a full spectrum of harmonics. This harmonic distortion adversely affects the network through degradation of the power quality, experienced by other operating resources connected to the affected transformer. Such harmonics can pose serious difficulties in designing filters [11].

4.1.3 Internal Resonances in the Windings

Due to the rapid reduction in its magnetizing impedance, caused by the saturation of the magnetic core, the transformer may become resonant with capacitive operating resources in the connected grid, e.g. cables or capacitor banks. This resonance between the transformer and capacitive operating resources is possible if the harmonic frequencies in the grid correspond to at least one of the resonant frequencies of the transformer. In this case local overvoltages and overcurrents are generated within the transformer windings. These internal resonances eventually degenerate into dielectric incidents, leading to transformer damage [16].

4.1.4 Increased Reactive Power Consumption

An effect which also can stem from core saturation is increased reactive power absorption. This can be explained by realizing that core saturation results in an increase in magnetization current, which is basically an inductive current. The increase in this inductive current will result in greater reactive power loss across the magnetizing reactance [17]. Thus, if the initial load current through the transformer is inductive (which is often the case) then the overall reactive power (VAR absorption) will increase due to the increased magnetizing current. If saturation is severe, the VAR absorption will become noticeable, along with an associated decrease in displacement power factor. This is a particularly undesirable feature, as it indicates increased losses [19].

4.1.5 Overheating

When a transformer enters the saturated region of operation due to a DC bias, extra harmonics are generated. These harmonics, with elevated frequency levels, encounter a greater resistance due to the skin effect. This in turn exacerbates heating effects by increased resistive losses [20]. Continuous saturation leads also to an increased localized stray flux heating [11].

4.1.6 Acoustic Noise Emissions

A transformer in a saturated operating point due to a DC bias will produce greater levels of acoustic noise. Studies have shown that relatively small levels of DC bias can cause the transformer to emit greater levels of noise. A certain number of mechanisms are responsible for the emission of this increased noise. Firstly, the Lorentz Force Acoustic Signal (LFAS) causes mechanical forces between the core laminations, hence inducing rattling and thus noise. This particular source of noise is largely dependent on the construction style of the transformer. Another form of noise stems from the rotation of magnetic domains. This source of noise becomes a concern when the transformer reaches saturation and the magnetostriction becomes large, wherefore a movement within the core laminations is experienced. These movements can lead to a deterioration of the interlamination insulation in the long run, while the emitted noise is particularly irritating to human beings [11, 21].

4.1.7 Corrosive Effects

Another negative effect of DC biased transformers is that corrosive effects are accelerated. The injection of DC currents can create ground currents which can rapidly corrode the operating resources [22].

4.1.8 Residual Magnetism

Due to injected DC currents, transformers can exhibit residual magnetism. This is particularly evident for transformers which have a tank. For small gaps between the tank and the transformer core, any residual magnetism can impact the magnetizing currents and hysteresis characteristic [23].

4.2 Instrument Transformers under DC Bias

As mentioned in the section about power transformers before, injected DC currents can lead to a saturation of the transformer's core. This effect is as well relevant for instrument transformers like current and potential transformers.

When current or potential transformers are used for protective aims, the saturation of the transformer's core may become critical. Most protective relays make their tripping decisions based on RMS values. If the signal supplied by the instrument transformer is distorted due to saturation of the transformer's core, the measurement of the RMS value will be lower than the actual value. This may lead to malfunctions of the protective relays like false tripping or a decreased sensitivity. For deep saturation of the transformer's core, the tripping of a protective relay can be prevented [11, 24]. Simulations show clearly that the larger the DC current is the sooner and deeper the current transformer's core enters its saturation region. The magnitude of the DC current which leads to saturation depends on the specific current transformer [25].

4.3 Effects on Converter

Induced fundamental frequency (50 Hz) currents in DC transmission lines cause a current ripple on the DC circuit. This leads to harmonics and a DC component in the converter transformer's secondary winding due to the converter's switching. This DC component can cause half-cycle saturation of the transformer, which results in the injection of a broad spectrum of harmonics at both sides of the converter [11]. Such harmonics may lead to excessive voltages due to harmonic resonances and the instability of the system [26]. The effects the transformer experiences are the same as stated in the section about power transformers under DC bias. These are e.g. an increased noise level, an increased heating and a decreased converter transformer lifetime.

Due to the previously mentioned DC current, the instrument transformer which measures the current in the secondary winding also experiences saturation. This leads to inaccurate measurement, which on the one hand affects the control of the converter negatively. On the other hand the differential protection of the transformer can be affected. It is recommended to keep the steady-state fundamental component of the DC current ripple below 0.1% of the converter rating to ensure a negligible influence on the system's performance. Otherwise the effect on converter performance has to be studied [11].

4.4 Mitigation Options

By avoiding a small separation distance between AC and DC transmission lines, the influence on each other can be lowered. Another option might be avoiding long distance parallel AC and DC transmission lines. Due to the fact that these approaches might not be feasible in any case, other options have to be utilized. For example, blocking filters and smoothing inductors might be applied in the DC circuits to attenuate the flow of fundamental frequency current into the converters [27]. The impact of such currents may also be limited by utilizing the control of the DC converters. But also overhead ground wires acting as a shield, the transposition of the AC and the DC transmission lines respectively and a compact arrangement of the conductors can limit the EMI between them [11, 28]. On the contrary does the increasing of the size of the converter transformer not have an effect on the saturation, it will be reached for any practical saturation level [11].

5 Conclusion, Outlook and Future Work

The aim of this project is the fundamental analysis of the mutual electromagnetic interference of parallel medium voltage AC and medium voltage DC overhead lines and cables. Such a parallel guide may results not only from technical, but also from economic and ecological reasons [29]. Basically the three coupling mechanisms capacitive coupling, inductive coupling and conductive coupling exist. By exemplary calculations it has been shown that at medium voltage overhead transmission lines no corona discharges occur due to the lower voltage compared to high voltage overhead lines, thus no conductive coupling has to be taken into account. An appropriate transmission line model has been selected, which takes capacitive and inductive coupling into account. Suitable solution methods provide accurate simulation results for steady-state and transient calculations. Due to the lack of a real interference route an exemplary interference route with exemplary parameters for the overhead transmission lines, cables as well as AC and DC voltages and currents in normal operating conditions and fault conditions has been considered. In this way, the method of analysis of EMI for such an interference route is illustrated. For this exemplary interference route, different arrangements of AC and DC overhead transmission lines and buried cables have been considered.

The steady-state results for the arrangements with only AC conductors have been presented and have been compared with the corresponding transient results. It has been showed that for some cases the voltages and currents at the ends of the conductors during the transients are larger than in steady-state. Therefore, in general, transient calculations have to be performed to examine the resulting maximum voltages and currents for the mutual electromagnetic interference of conductors in a given interference route. The transient results for the arrangements with DC conductors only have been presented as well. The results for AC and DC show that the maximum coupling occurs between the conductors of overhead lines. But also the coupling between overhead lines and buried cables as well as between cables cannot be neglected for the considered exemplary arrangements. Of course the distance between the conductors plays an important role regarding the strength of the mutual coupling. Furthermore, for analysis of the fault conditions the choice of the fault affected phases in the arrangements has an influence on the strength of the mutual coupling. Therefore, the worst case conditions should be determined by selecting the fault affected phases appropriately.

Injected currents and induced voltages can have a negative influence on other operating resources in the neighborhood of the influenced conductors due to an influence on the regular voltage and current waveforms. For example for transformers, induced DC currents lead to a

saturation of the transformer's core. This can lead not only to the transformer being a source of harmonics, but also to an increased noise and overheating, which is a potential thread for a power transformer's longevity. For instrument transformers a saturation of the core leads to distorted measurements which can prevent relays from tripping or lead to false tripping. Therefore it might be necessary to review the AC protection system for AC grids with DC circuits in the close neighborhood [27]. Converters experience similar effects, their transformer's core can saturate and the converter itself can become a source of harmonics. The strength of the coupling between the conductors, thus the magnitude of the injected currents and induced voltages, can be lowered by mitigation options, which are briefly presented. One example for such a mitigation option is the usage of earth wires for overhead transmission lines.
For unipolar DC lines with earth return or for bipolar DC lines with earth return in unsymmetrical operating conditions, earth currents will flow. This has to be taken into account due to the fact that such earth currents can lead to corrosion of metallic components like pipes in the flow direction of the earth currents. Transient ground currents also induce currents in neighboring conductors as long as the steady-state has not been reached. The current magnitude is not affected very much by line distance, grounding resistance or the presence of ground wires [30].

It has been assumed that the considered DC interference route is part of a large, meshed DC grid. Therefore the DC voltages and currents at the ends of the influencing conductors have been modeled with ideal voltage and current sources. For much smaller grids the influence of the converters and their control algorithms can be taken into account by modeling the whole grid or the most relevant parts of it. This should be done by modeling the converters in more detail instead of just using ideal voltage and current sources at the ends of the transmission lines. Furthermore, by modeling at least the neighboring grid of the interference route and by using a given load flow situation, different fault locations and their influence on the mutual coupling can be analyzed instead of presetting the fault currents in the influencing conductors by using ideal current sources. It can be summarized that for every parallel operation of medium voltage AC and DC overhead lines and/or cables the transient mutual electromagnetic interference has to be investigated.

In literature it is stated that the voltage at an arbitrary position on a conductor can be larger than the voltages at the ends of the conductor [31]. With the steady-state simulation software used in this project it is possible to calculate the voltage profiles for AC on the conductors. But with the used transient simulation software it is only possible to calculate the transient voltages

for AC and DC at the ends of the conductors. But as the results show, during the transients the voltages may exceed their steady-state values. Splitting up the transmission line in many small segments for calculating the voltages at many positions on the conductors is no alternative due to the fact that errors will sum up, which decreases the accuracy of the simulation significantly [31]. Therefore it is recommended to develop a software tool which allows to calculate the transient voltage at arbitrary positions (the voltage profile) on the conductors of a given conductor arrangement without artificial segmentation of the transmission line. This could be realized as a shorter follow-up seed fund project.

6 Bibliography

[1] P. S. Maruvada, „Corona-Generated Space Charge Environment in the Vicinity of HVDC Transmission Lines,“ *IEEE Transactions on Electrical Insulation,* Bd. 17, Nr. 2, pp. 125-130, 1982.

[2] M. Kizilcay, A. Agdemir und M. Lösing, „Interaction of a HVDC System with 400-kV AC Systems on the Same Tower,“ in *International Conference on Power System Transients*, 2009.

[3] A. Küchler, Hochspannungstechnik, Springer Verlag, 2009.

[4] P. S. Maruvada, Corona in transmission systems, Johannesburg: Crown Publ., 2011.

[5] K. Heuck, K.-D. Dettmann und D. Schulz, Elektrische Energieversorgung, Vieweg Teubner, 2010.

[6] P. S. Maruvada und S. Drogi, „Field and ion interactions of hybrid AC/DC transmission lines,“ *IEEE Transactions on Power Delivery,* Bd. 3, Nr. 3, pp. 1165-1172, 1988.

[7] Manitoba HVDC Research Centre, EMTDC User's Guide, Winnipeg, Manitoba, Canada, 2010.

[8] RTDS Technologies, RTDS overhead line constants manual, Winnipeg, Manitoba, Canada, 2014.

[9] A. Wasserrab, B. Just und G. Balzer, „Contribution of HVDC converters to the DC short circuit current,“ *48th International Universities' Power Engineering Conference (UPEC),* 2013.

[10] R. T. Pinto, Multi-terminal DC networks, Ph.D. thesis, TU Delft, Delft, 2014.

[11] E. V. Larsen, R. A. Walling und C. J. Bridenbaugh, „Parallel AC/DC transmission lines steady-state induction issues,“ *IEEE Transactions on Power Delivery,* Bd. 4, Nr. 1, pp. 667-674, 1989.

[12] T. Dong, Modulares Analysesystem für Grundsatzuntersuchungen an langen Netzverbindungen mit Drehstrom-Hoch- und Höchstspannungskabeln, Ph.D. thesis, University Duisburg-Essen, Germany, 2012.

[13] R. Verdolin, A. M. Gole, E. Kuffel, N. Diseko und B. Bisewski, „Induced overvoltages on an AC-DC hybrid transmission system,“ *IEEE Transactions on Power Delivery,* Bd. 10, Nr. 3, pp. 1514-1524, 1995.

[14] L. Cao, Study on the influence of DC biasing current on power transformer magnetization characteristics, Ph.D. thesis, Tsinghua University, Beijing, 2007.

[15] P. Picher, L. Bolduc, A. Dutil und V. Q. Pham, „Study of the acceptable DC current limit in core-form power transformers,“ *IEEE Transactions on Power Delivery,* Bd. 12, Nr. 1, pp. 257-265, 1997.

[16] Schneider Electrics, Effect of direct current on transformers.

[17] P. R. Price, „Geomagnetically induced current," *IEEE Transactions on Power Delivery,* Bd. 17, Nr. 4, pp. 1002-1008, 2002.

[18] M. T. Bishop, J. F. Baranowski, D. Heath und S. J. Benna, „Evaluating harmonic-induced transformer heating," *IEEE Transactions on Power Delivery,* Bd. 11, Nr. 1, pp. 305-311, 1996.

[19] A. K. Zeimer, The effect of DC current on power transformers, Ph.D. thesis, University of Southern Queensland, 2000.

[20] S. Lu, Y. Liu und J. De La Ree, „Harmonics generated from a DC biased transformer," *IEEE Transactions on Power Delivery,* Bd. 8, Nr. 2, pp. 725-731, 1993.

[21] F. De Leon, V. Tatu und M. Van der Veen, „Measuring acoustic noise emitted by power transformers," in *AES 109th Convention*, Los Angeles.

[22] G. Ledwich und K. Masseur, „Grid connection without mains frequency transformers," *Journal of Electrical and Electronics Engineering,* Bd. 19, Nr. 1, pp. 31-36, 1999.

[23] E. F. Fuchs, D. J. Roesler und Y. You, „Modeling and simulation and their validation of three-phase transformers with three legs under DC bias," *IEEE Transactions on Power Delivery,* Bd. 14, Nr. 2, pp. 443-449, 1999.

[24] C. Li, Q. Li, J. Yao und M. Liu, „The characteristics of electromagnetic current transformers with DC bias," in *Sustainable Power Generation and Supply*, Nanjing, 2009.

[25] J. D. Aspnes und R. P. Merritt, „Effect of DC excitation on instrument transformers," *IEEE Transactions on Power Apparatus and Systems,* Bd. 102, Nr. 11, pp. 3706-3712, 1983.

[26] J. Z. Zhou, R. S. Burton, D. E. Fletcher und J. B. Davies, „Coupling between DC lines with a neutral conductor and parallel AC lines," in *International IET Conference on AC and DC Power Transmission*, 2010.

[27] D. A. Halamay, K. M. Saxby, J. L. Bala und R. Spacek, „Feasibility study of a high-voltage DC & AC multi-circuit hybrid transmission line," in *Proceedings of the 37th Annual North American Power Symposium*, 2005.

[28] J. Tang, R. Zeng, H. Ma, J. He, J. Zhao, X. Li und Q. Wang, „Analysis of electromagnetic interference on DC line from parallel AC line in close proximity," *IEEE Transactions on Power Delivery,* Bd. 22, Nr. 4, pp. 2401-2408, 2007.

[29] J. Ulleryd, M. Ye und G. Moreau, „Fundamental frequency coupling between HVAC and HVDC lines in the Quebec-New England multiterminal system-comparison between field measurements and EMTDC simulations," *Proceedings of International Conference on Power System Technology,* Bd. 1, pp. 498-502, 1998.

[30] N. Chopra, A. M. Gole, J. Chand und R. W. Haywood, „Zero sequence currents in AC lines caused by transients in adjacent DC line," *IEEE Transactions on Power Delivery,* Bd. 3, Nr. 4, pp. 1873-1879, 1988.

[31] L. Marti und H. W. Dommel, „Calculation of voltage profiles along transmission lines," *IEEE Transactions on Power Delivery,* Bd. 12, Nr. 2, pp. 993-998, 1997.

7 List of Tables and Figures

Figure 1: Capacitive interference on line $\boldsymbol{I1}$ caused by circuit 1 depending on the distance between $\boldsymbol{I1}$ and $\boldsymbol{W1}$ 5

Figure 2: Inductive interference on line $\boldsymbol{I1}$ caused by circuit 1 depending on the distance between $\boldsymbol{I1}$ and $\boldsymbol{W1}$ 6

Figure 3: Investigated DC overhead line arrangement 7

Figure 4: Input parameters for the calculation of p and q 8

Figure 5: Conductor arrangement for analysis of DC corona discharges 11

Figure 6: Equivalent circuit of infinitesimal short transmission line segment 14

Figure 7: Examined interference route 17

Figure 8: Overhead line – overhead line arrangements 18

Figure 9: Overhead line – cable arrangements 19

Figure 10: Cable – overhead line arrangements 19

Figure 11: Cable – cable arrangements 20

Figure 12: Coupled voltages in normal operating conditions (AC overhead line – overhead line) 25

Figure 13: Coupled currents in normal operating conditions (AC overhead line – overhead line) 25

Figure 14: Coupled voltages in normal operating conditions (AC overhead line – cable) 26

Figure 15: Coupled currents in normal operating conditions (AC overhead line – cable) 26

Figure 16: Coupled voltages in fault conditions (AC overhead line – overhead line) 27

Figure 17: Coupled currents in fault conditions (AC overhead line – overhead line) 27

Figure 18: Coupled voltages in fault conditions (AC overhead line – cable) 28

Figure 19: Coupled currents in fault conditions (AC overhead line – cable) 28

Figure 20: Coupled transient voltages in normal operating conditions (AC overhead line - overhead line) for both sides isolated 32

Figure 21: Coupled transient currents in normal operating conditions (AC overhead line - overhead line) for both sides grounded 33

Figure 22: Coupled transient voltages in normal operating conditions (AC cable - cable) for both sides isolated 34

Figure 23: Coupled transient voltages in fault conditions (AC overhead line - overhead line) for one side grounded 35

Figure 24: Coupled transient currents in fault conditions (AC overhead line - overhead line) for both sides grounded 36

Figure 25: Coupled transient currents in fault conditions (AC cable - overhead line) for both sides grounded 37

Figure 26: Coupled transient voltages in fault conditions (AC cable - cable) for one side grounded 38

Figure 27: Coupled transient currents in fault conditions (AC cable - cable) for both sides grounded 39

Figure 28: Coupled transient voltages in normal operating conditions (DC overhead line – overhead line) for both sides isolated 42

Figure 29: Coupled transient currents in normal operating conditions (DC overhead line – overhead line) for both sides grounded 43

Figure 30: Coupled transient voltages in normal operating conditions (DC cable - cable) for both sides isolated 44

Figure 31: Coupled transient currents in normal operating conditions (DC cable - cable) for both sides grounded 45

Figure 32: Coupled transient voltages in fault conditions (DC overhead line - overhead line) for both sides isolated 46

Figure 33: Coupled transient currents in fault conditions (DC overhead line - overhead line) for both sides grounded 47

Figure 34: Coupled transient voltages in fault conditions (DC overhead line - cable) for one side grounded 48

Figure 35: Coupled transient currents in fault conditions (DC overhead line - cable) for both sides grounded 49

Table 1: Utilization factor depending on parameters p and q 9

Table 2: Maximum DC electrical field strengths at conductors' surface of analyzed arrangement 12

Table 3: Relevant coupling mechanisms between medium voltage lines in steady state conditions 12

Table 4: Relevant coupling mechanisms between medium voltage lines in transient conditions 13

Table 5: Considered arrangements 17

Table 6: Parameters of the aerial conductors 20

Table 7: Parameters of the cable layers 21

Table 8: Fault afflicted phases in the considered arrangements 23

Table 9: Examined arrangements for steady state EMI 24

Table 10: Maximum rms steady-state voltages and currents in normal operating conditions and fault conditions for AC 29

Table 11: Maximum transient rms and peak voltages and currents in normal operating conditions and fault conditions for AC 40

Table 12: Examined DC arrangements for transient EMI 41

Table 13: Maximum transient peak voltages and currents in normal operating conditions and fault conditions for DC 50

Flexible Elektrische Netze FEN GmbH

Campus-Boulevard 57
52074 Aachen
Germany

T +49 241 80 22471
info@FENaachen.net
www.FENaachen.net